Chromium biogeochemistry and stable isotope distribution in the Southern Ocean

Journal Article

Author(s):
Rickli, Jörg; Janssen, David J.; Hassler, Christel; Ellwood, Michael J.; Jaccard, Samuel L.

Publication date:
2019-10-01

Permanent link:
https://doi.org/10.3929/ethz-b-000367419

Originally published in:
Geochimica et Cosmochimica Acta 262, https://doi.org/10.1016/j.gca.2019.07.033

Available online at www.sciencedirect.com

ScienceDirect

Geochimica et Cosmochimica Acta 262 (2019) 188–206

Geochimica et Cosmochimica Acta

www.elsevier.com/locate/gca

Chromium biogeochemistry and stable isotope distribution in the Southern Ocean

Jörg Rickli [a,b,*], David J. Janssen [a], Christel Hassler [c], Michael J. Ellwood [d], Samuel L. Jaccard [a]

[a] University of Bern, Institute of Geological Sciences & Oeschger Center for Climate Change Research, Baltzerstrasse 1-3, 3012 Bern, Switzerland
[b] ETH Zurich, Institute of Geochemistry and Petrology, Clausiusstrasse 25, 8092 Zurich, Switzerland
[c] Department F.-A. Forel for Environmental and Aquatic Sciences, University of Geneva, Boulevard Carl-Vogt 66, 1211 Geneva, Switzerland
[d] Research School of Earth Sciences, Australian National University, Canberra, ACT 2601, Australia

Received 16 March 2019; accepted in revised form 17 July 2019; available online 26 July 2019

Abstract

Despite the potential of stable chromium (Cr) isotope compositions as a proxy for past changes in oceanic redox conditions, a detailed understanding of the processes that govern their spatial distribution in the modern ocean is still lacking. Here, we report seawater Cr isotope compositions and concentrations from the uppermost 1000 m of the water column in the Southern Ocean. The survey includes a cross-frontal transect from Tasmania to Antarctica, sites near the Antarctic ice-edge and in the vicinity of the Balleny Islands, as well as sites in the Drake Passage.

Although a coastal influence is clearly visible in the silicon-nitrate relationship at the stations neighbouring the Balleny Islands, close to the Mertz Glacier and adjacent to the western Antarctic Peninsula, seawater δ^{53}Cr and Cr concentrations remain largely unaffected. As for the coastal sites, Cr depletion and isotopic shifts are also virtually absent in Antarctic and Subantarctic surface waters of the open ocean. Biological uptake of Cr and/or scavenging of Cr onto sinking particles are apparently not strong enough to induce water column variability. Contrasting with the small variations in δ^{53}Cr and Cr concentrations at each site, there are, however, systematic meridional changes. The seawater samples show an increase in Cr concentrations and a parallel decrease in δ^{53}Cr southwards from the Subantarctic across the Polar Frontal into the Antarctic Zone. Chromium concentrations and δ^{53}Cr are, however, uniform at all stations south of the Polar Front. The spatial pattern is consistent with the mixing of Southern Ocean sourced Cr with an isotopically heavier Cr pool from northward of the studied area, as evidenced by strong correlations of Cr and δ^{53}Cr with salinity at the level of Subantarctic Mode Water and at shallower levels. The heavy δ^{53}Cr signature of the northerly Cr pool could either result from Cr cycling in the subtropical gyre or originate in oxygen minimum zones. On a regional scale, δ^{53}Cr is strongly correlated with phosphate concentrations, which may hint at a time-integrated effect of major nutrient drawdown on δ^{53}Cr.

Southern Ocean data support previous work demonstrating a strong relationship between seawater Cr concentrations and δ^{53}Cr. At the studied sites, this relationship reflects mixing of isotopically distinct Cr pools. The end-members observed in the studied area are, however, consistent with the previously described closed-system Rayleigh type fractionation of Cr in seawater characterized by a single fractionation factor. The underlying processes, which produce the observed fractionation, are not fully constrained to date.

Keywords: Seawater; Chromium isotopes; Southern Ocean

* Corresponding author at: ETH Zurich, Institute of Geochemistry and Petrology, Clausiusstrasse 25, 8092 Zurich, Switzerland.
E-mail address: joerg.rickli@erdw.ethz.ch (J. Rickli).

https://doi.org/10.1016/j.gca.2019.07.033
0016-7037/

1. INTRODUCTION

Chromium isotope records have been used to infer past redox conditions of the oceans and the oxygenation of the atmosphere (Frei et al., 2009; Crowe et al., 2013; Planavsky et al., 2014). In addition, a link may also exist between seawater Cr isotope variations and changes in the export of organic matter from the oceans (Connelly et al., 2006; Scheiderich et al., 2015; Semeniuk et al., 2016). Although stable Cr isotopes have been used as a paleoproxy to identify changes in the Earth surface environment (e.g. Frei et al., 2009), our current understanding of the processes that govern the biogeochemical cycling of Cr isotopes in seawater and their spatial variability is limited. In order to better understand the marine Cr cycle, improved constraints on the oceanic inputs and sinks of Cr, as well as on the controls of its internal cycling in variable oceanic settings are needed.

Chromium has two stable oxidation states at Earth surface conditions, namely Cr(III) and Cr(VI) (e.g. Fendorf, 1995; Bonnand et al., 2013). Chromium (VI) is soluble and accounts for 75–95% of total dissolved Cr in seawater (Sirinawin et al., 2000). Chromium(III), on the other hand, is particle reactive and forms insoluble chromium hydroxide compounds (Fendorf, 1995). During Cr(VI) reduction, isotope fractionation occurs with an enrichment of light Cr isotopes in the reduced Cr species (e.g. Ellis et al., 2002).

The isotopic fractionation factor of Cr (α) associated with a chemical reaction is determined by the ratio of $^{53}Cr/^{52}Cr$ in the product to $^{53}Cr/^{52}Cr$ in the reactant. For convenience, the isotopic fractionation factor is often reported as an isotopic enrichment factor ε (Eq. (1)), which equates to the difference in the isotope ratios of the product and the reactant, expressed in δ-notation relative to the standard reference material NIST 979 (Eq. (2)):

$$\varepsilon[‰] = (\alpha - 1) \times 1000 \approx \delta^{53}Cr_{product} - \delta^{53}Cr_{reactant} \quad (1)$$

$$\delta^{53}Cr_{\,sample}[‰] = \frac{\left(\frac{^{53}Cr}{^{52}Cr}\right)_{sample} - \left(\frac{^{53}Cr}{^{52}Cr}\right)_{NIST\ 979}}{\left(\frac{^{53}Cr}{^{52}Cr}\right)_{NIST\ \ 979}} \times 1000 \quad (2)$$

A range of Cr reducing processes are known, including reduction by dissolved Fe(II) (Døssing et al., 2011; Kitchen et al., 2012), organic substances (Kitchen et al., 2012), bacteria (Sikora et al., 2008; Basu et al., 2014) and H_2O_2 (Zink et al., 2010) with associated isotopic enrichment factors ranging between −2.2 and −5‰. The high redox potential of the Cr(VI)/Cr(III) couple, on the other hand, limits the agents capable of oxidizing Cr(III) in seawater. Oxidation is slow and is mainly linked to the interaction with Mn-oxides (van der Weijden and Reith, 1982; Saleh et al., 1989), and the associated fractionation is relatively small (Zink et al., 2010).

δ^{53}Cr seawater values range between +0.4 and +1.7‰ (Bonnand et al., 2013; Scheiderich et al., 2015; Goring-Harford et al., 2018; Moos and Boyle, 2019) and are offset towards heavy Cr isotope compositions relative to magmatic rocks ($\delta^{53}Cr = -0.12 \pm 0.1$‰, Schoenberg et al., 2008). The offset from magmatic rocks is expected, as rivers constitute the predominant source of Cr in seawater (76–98%, Jeandel and Minster, 1987; Bonnand et al., 2013; McClain and Maher, 2016) and oxidative weathering of Cr(III) and subsequent back-reduction results in isotopically heavy Cr in streams and rivers (Farkaš et al., 2013; Frei et al., 2014; D'Arcy et al., 2016). There are, at present, relatively few constraints about the isotope compositions of the potential Cr sinks. Iron manganese crusts, for instance, represent an isotopically light sink, but are associated with minor Cr fluxes (Wei et al., 2018). Recent studies have highlighted removal of dissolved Cr in reducing sediments (Reinhard et al., 2014; Gueguen et al., 2016), potentially catalysed by ferrous iron (Bauer et al., 2018).

In contrast to other redox sensitive elements, for instance molybdenum (seawater residence time of ~440 kyr, Miller et al., 2011), Cr has a relatively short seawater residence time, possibly as low as 3–10 kyr (Whitfield and Turner, 1987; McClain and Maher, 2016). As a result, Cr isotopes may yield information on oceanic redox changes on time scales similar to global ocean mixing both under modern conditions as well as in the geologic past (e.g. Gueguen et al., 2016). On the other hand, unlike molybdenum, oceanic δ^{53}Cr is spatially variable, and therefore variations of seawater Cr isotopes at a given location through time will reflect changes in local and/or global conditions.

With the exception of one study (X. Wang et al., 2019), all currently published δ^{53}Cr seawater data represent total dissolved Cr, hence the isotope composition of the combined Cr(III) and Cr(VI) pools. The first published δ^{53}Cr profile stems from the Argentine Basin and includes the lowest δ^{53}Cr values reported thus far (as low as +0.4‰; Bonnand et al., 2013). Neither Cr concentrations, nor δ^{53}Cr reveal much variability in the sampled depth interval between 30 and 2300 m, suggesting that there is little vertical redistribution in oligotrophic settings. However, it should be noted that the samples were not filtered upon collection (Bonnand et al., 2013). As a result, there are some concerns about the integrity of the data (Goring-Harford et al., 2018). Scheiderich et al. (2015) reported δ^{53}Cr data from the Beaufort Sea in the Arctic Ocean, complemented by a few Atlantic and Pacific water samples. The composite profile from the Beaufort Sea shows a gradual increase in Cr concentrations and a concomitant decrease in δ^{53}Cr down to a depth of ~500 m, below which there is little variability. This nutrient-like shape likely results from the mixing of Pacific- and Atlantic-sourced waters rather than Cr depletion in the surface and release at depth (Scheiderich et al., 2015). A compilation of all available data at the time showed that the global δ^{53}Cr distribution can be viewed as a closed system Rayleigh fractionation associated with processes that yield an isotopic enrichment factor close to −0.8‰ (Scheiderich et al., 2015). Recent studies have addressed the behaviour of Cr and its isotopes in oxygen deficient waters. Goring-Harford et al. (2018) studied sites in the open subtropical Atlantic Ocean characterized by dysoxic conditions (oxygen concentrations as low as 44 μmol/kg), but found little evidence for the reduction and subsequent scavenging of Cr from solution. In contrast, lowered Cr concentrations

and relatively heavy $\delta^{53}Cr$ values on the Senegalese shelf indicate that reduction and removal of Cr may be associated with high primary productivity and particle export flux. Similar to the open ocean subtropical Atlantic sites, Cr reduction does not appear to occur at the SAFe station in the North Pacific (oxygen concentrations as low as 13.2 μmol/kg). The heaviest Cr isotope compositions at 200 m water depth at SAFe could, however, reflect advected Cr from the oxygen-deficient zone of the Eastern Tropical North Pacific (Moos and Boyle, 2019). Reduction of Cr(VI) has previously been documented in this region (Rue et al., 1997).

In general, the degree of nutrient-like behaviour of Cr in seawater remains debated (see for instance Whitfield and Turner, 1987; Sirinawin et al., 2000; Bonnand et al., 2013; Moos and Boyle, 2019). Based on concentration measurements alone, it has been accepted that Cr is not fully conservative (e.g. Sirinawin et al., 2000), consistent with the aforementioned isotopic variability. Chromium often shows surface ocean depletions that are, however, relatively subtle (e.g. Jeandel and Minster, 1987).

This contribution is concerned with the modern-day distribution of Cr isotopes in seawater, which has not been explored in much detail so far (Bonnand et al., 2013; Scheiderich et al., 2015; Paulukat et al., 2016; Goring-Harford et al., 2018; Moos and Boyle, 2019). More specifically, we explore the distribution of Cr concentrations and isotope compositions in the biogeochemically diverse region of the Southern Ocean.

2. OCEANOGRAPHIC SETTING

2.1. Southern Ocean circulation

The eastward-flowing Antarctic Circumpolar Current (ACC) dominates ocean circulation in the Southern Ocean, broadly defined as the region between Antarctica and the Subtropical Fronts (STFs, Talley et al., 2011). The ACC, reaching from the surface to great depth, is constrained to the north by the Subantarctic Front (SAF) and to the south by its southern boundary (Fig. 1; Orsi et al., 1995). Within the ACC there are three distinct fronts, the SAF, the Polar Front (PF) and the Southern ACC Front. The region between the STF and the SAF is referred to as the Subantarctic Zone (SAZ) and comprises the poleward fraction of the subtropical gyres. Between the fronts of the ACC are three zones of slower eastward flow, the Polar Frontal Zone (PFZ) between the SAF and PF, the Antarctic Zone (AZ) between the PF and Southern ACC Front, and the Southern Zone between the Southern ACC Front and the southern boundary (Orsi et al., 1995).

Westerly winds drive northward Ekman transport in the latitudes of the SAF and PF, which is compensated for by upwelling of nutrient-rich Upper Circumpolar Deep Water (UCDW) (e.g. Talley et al., 2011). A fraction of the upwelled water is transported northwards, where it is in part subducted at the SAF to form Subantarctic Mode and Antarctic Intermediate Waters (SAMW, AAIW). Southward transported waters are altered by intense winter cooling and

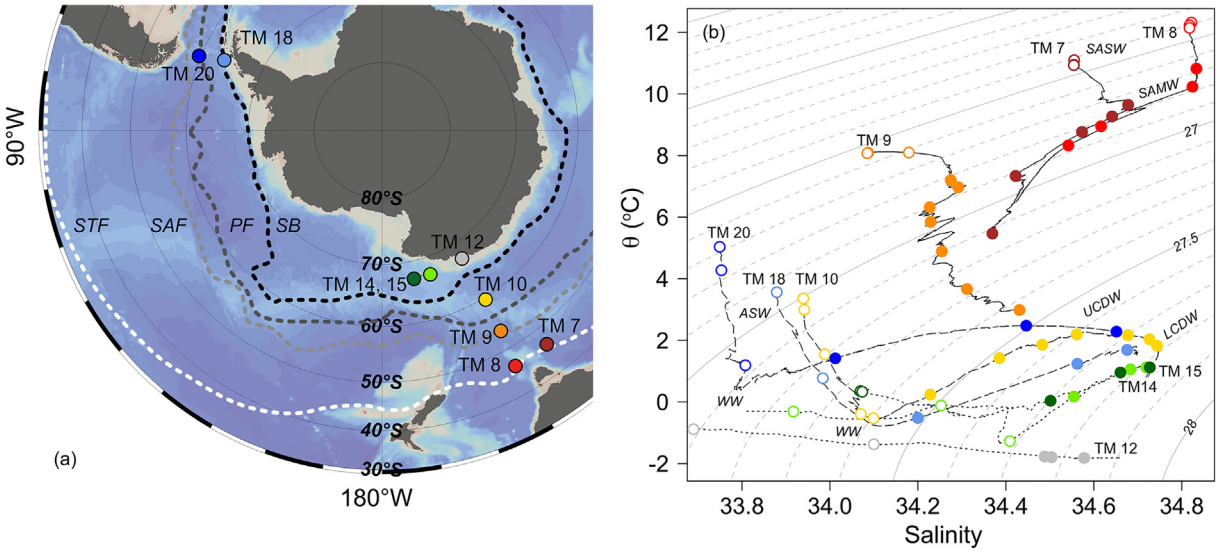

Fig. 1. (a) Overview of sampled stations in the Southern Ocean with respect to the major fronts (Orsi et al., 1995). STF: Subtropical Front, SAF: Subantarctic Front, PF: Polar Front; SB: southern boundary of the ACC. The ACC is constrained in the north by the SAF and in the south by its southern boundary. (b) Relationship between potential temperature (θ) and salinity (Henry et al., 2019; see caption to Table 1). Sampled surface water masses include Subantarctic Surface (SASW) and Antarctic Surface Water (ASW) including its densest variety Winter Water (WW). At the northern stations 7 and 8 Subantarctic Mode Water (SAMW) occupies intermediate levels, whereas Upper and/or Lower Circumpolar Waters (U/LCDW) prevail below the surface waters at the more southerly stations. For more details see Section 2. Open circles represent surface waters (ASW, SASW), filled circles all deeper water masses. Note that the two shallowest samples at station 12 are outside the displayed salinity range.

Table 1
Hydrographic and Cr data for the studied samples (Henry et al., 2019; Rickli et al., 2019). The uncertainty on the Cr isotope values is ±0.036‰ and ±2.2% for Cr concentrations (2 SD) based on full replicate measurements of OSIL waters and two ACE samples (Table 3, Section 3.2.4.4). Temperature (in situ), salinity and oxygen data were extracted from the CTD at ACE stations neighbouring the trace metal sampling sites (Leg 1, CTD cast 12; Leg 2, CTD casts 1, 3, 5, 13, 22, 23, 33, 35; Henry et al., 2019). Oxygen data were not calibrated and reflect raw sensor data, contrasting with calibrated salinity and temperature (Henry et al., 2019). Potential temperature, potential density and neutral density were calculated in Ocean Data View (Schlitzer, 2019).

Station	Depth (m)	Potential Temp. (°C)	Salinity	O_2 (μmol/kg)	Cr (nmol/kg)	δ^{53}Cr (‰)	Int. error 2 SEM (‰)	Potential density (kg/m^3)	Neutral density (kg/m^3)	Water mass
TM 7	15	11.10	34.555	249	3.28	1.02	0.02	26.42	26.47	SASW
46.906 S	40	10.95	34.555	248	3.27	1.04	0.02	26.44	26.50	SASW
141.931 E	60	10.93	34.554	250	3.27	1.05	0.02	26.44	26.50	SASW
	150	9.64	34.678	243	3.27	1.06	0.02	26.76	26.84	SAMW
	250	9.27	34.642	244	3.27	1.05	0.02	26.80	26.88	SAMW
	500	8.77	34.573	234	3.31	1.03	0.02	26.82	26.92	SAMW
	750	7.34	34.422	210	3.39	0.99	0.03	26.92	27.03	SAMW/AAIW
	1000	5.47	34.369	185	3.52	0.98	0.02	27.12	27.26	SAMW/AAIW
TM 8	15	12.32	34.822	251	3.22	1.04	0.02	26.39	26.44	SASW
46.393 S	40	12.23	34.818	249	3.23	1.05	0.03	26.41	26.46	SASW
150.389 E	60	12.14	34.817	246	3.22	1.05	0.03	26.42	26.47	SASW
	150	10.82	34.833	241	3.22	1.06	0.02	26.68	26.75	SASW/SAMW
	250	10.23	34.824	242	3.22	1.05	0.02	26.78	26.86	SAMW
	500	8.95	34.617	234	3.30	1.02	0.02	26.83	26.92	SAMW
	750	8.33	34.542	238	3.30	1.02	0.02	26.87	26.97	SAMW/AAIW
TM 9	15	8.09	34.087	271	3.45	0.99	0.03	26.55	26.61	(PFZ)
53.583 S	30	8.08	34.085	272	3.44	0.98	0.02	26.55	26.61	(PFZ)
149.298 E	50	8.10	34.179	270	3.44	0.97	0.02	26.62	26.69	(PFZ)
	80	7.20	34.275	265	3.40	0.99	0.03	26.82	26.92	(PFZ)
	125	6.97	34.292	259	3.37	1.00	0.02	26.87	26.97	(PFZ)
	200	6.32	34.227	257	3.41	0.97	0.02	26.90	27.02	(PFZ)
	300	5.84	34.229	242	3.46	0.99	0.02	26.97	27.09	(PFZ)
	500	4.89	34.255	213	3.52	0.96	0.02	27.10	27.25	(PFZ)
	750	3.67	34.312	191	3.64	0.93	0.02	27.28	27.45	(PFZ)
	1000	2.99	34.431	168	3.76	0.90	0.02	27.44	27.64	UCDW
TM 10	15	3.36	33.940	306	3.71	0.93	0.03	27.01	27.16	ASW
59.611 S	30	2.99	33.942	308	3.73	0.90	0.02	27.04	27.20	ASW
148.640 E	50	1.54	33.988	317	3.73	0.93	0.03	27.20	27.38	ASW
	80	−0.39	34.070	323	3.74	0.91	0.02	27.38	27.60	ASW, WW
	100	−0.53	34.099	318	3.74	0.93	0.03	27.41	27.64	ASW, WW
	125	0.24	34.228	270	3.75	0.92	0.02	27.47	27.71	ASW/UCDW
	150	1.42	34.385	208	3.76	0.92	0.02	27.53	27.77	ASW/UCDW
	200	1.85	34.483	177	3.80	0.90	0.02	27.57	27.81	UCDW
	250	2.20	34.561	161	3.81	0.93	0.02	27.61	27.84	UCDW
	500	2.17	34.678	164	3.86	0.90	0.02	27.71	27.94	UCDW/LCDW
	750	2.04	34.726	171	3.83	0.91	0.02	27.76	28.00	UCDW/LCDW
	1000	1.83	34.744	178	3.87	0.91	0.03	27.79	28.03	LCDW

(*continued on next page*)

Table 1 (*continued*)

Station	Depth (m)	Potential Temp. (°C)	Salinity	O_2 (μmol/kg)	Cr (nmol/kg)	δ^{53}Cr (‰)	Int. error 2 SEM (‰)	Potential density (kg/m^3)	Neutral density (kg/m^3)	Water mass
TM 12	15	−0.85	32.829	372	3.68	0.89	0.02	26.39	26.43	ASW
67.189 S	25	−1.04	32.923	370	3.66	0.91	0.03	26.48	26.53	ASW
145.721 E	50	−0.88	33.690	368	3.78	0.90	0.03	27.09	27.26	ASW
	80	−1.37	34.100	340	3.82	0.89	0.02	27.44	27.68	ASW
	150	−1.77	34.488	283	3.83	0.89	0.02	27.77	28.05	modified LCDW
	250	−1.79	34.504	283	3.83	0.92	0.02	27.78	28.31	modified LCDW
	500	−1.82	34.578	282	3.86	0.90	0.02	27.85	28.42	modified LCDW
TM 14	15	−0.31	33.917	323	3.78	0.93	0.02	27.25	27.44	ASW
67.290 S	40	−0.12	34.252	292	3.80	0.92	0.02	27.51	27.76	ASW
163.536 E	100	−1.27	34.409	254	3.82	0.92	0.03	27.69	27.95	ASW, WW
	150	0.17	34.555	216	3.82	0.92	0.03	27.74	28.01	LCDW
	250	1.06	34.683	190	3.87	0.90	0.03	27.79	28.06	LCDW
	500	1.12	34.719	185	3.92	0.90	0.03	27.82	28.10	LCDW
TM 15	15	0.35	34.069	308	3.80	0.91	0.02	27.34	27.55	ASW
67.100 S	50	0.33	34.074	307	3.80	0.92	0.02	27.35	27.56	ASW
167.360 E	100	0.04	34.502	213	3.85	0.92	0.02	27.71	27.97	ASW/LCDW
	150	0.96	34.661	182	3.88	0.90	0.03	27.78	28.04	LCDW
	500	1.12	34.727	180	3.95	0.89	0.03	27.82	28.11	LCDW
TM 18	15	3.56	33.879	302	3.74	0.89	0.02	26.94	27.07	ASW
63.963 S	50	0.77	33.984	301	3.77	0.89	0.02	27.25	27.45	ASW
66.242 W	100	−0.52	34.200	253	3.80	0.88	0.02	27.49	27.73	WW/UCDW
	180	1.24	34.562	173	3.86	0.87	0.02	27.68	27.92	UCDW
	300	1.69	34.676	164	3.88	0.91	0.02	27.74	27.98	UCDW/LCDW
TM 20	15	5.04	33.749	288	3.65	0.93	0.02	26.68	26.75	ASW
59.600 S	60	4.27	33.753	295	3.68	0.94	0.02	26.77	26.86	ASW
67.919 W	125	1.19	33.808	314	3.61	0.93	0.02	27.08	27.25	ASW/WW
	250	1.41	34.012	269	3.66	0.93	0.02	27.23	27.43	ASW/UCDW
	580	2.48	34.446	167	3.80	0.90	0.02	27.49	27.71	ASW/UCDW
	1000	2.28	34.651	158	3.87	0.89	0.02	27.67	27.89	UCDW

sea-ice formation, in particular on the Weddell and Ross Sea shelves. As a result, dense waters are formed and sink, leading to additions to Lower Circumpolar Deep Water (LCDW) and the formation of Antarctic Bottom Water (Orsi et al., 1999).

2.2. Antarctic circumnavigation expedition – studied stations and water masses

Seawater samples were collected during the Antarctic Circumnavigation Expedition (ACE) onboard the R/V *Akademik Tryoshnikov* between January and mid February 2017. The sample stations include a north-south, cross-frontal transect (TM 7–12) from south of Tasmania (TM 7, 8) to Mertz Glacier in Antarctica (TM 12), one station west and east of the Balleny Islands (TM 14 and 15, respectively) and two stations in the Drake Passage (TM 18, 20) (Fig. 1a, Table 1). ACE samples were obtained from the uppermost 1000 m of the water column, given the expectation that mostly surface ocean processes will affect seawater Cr.

Stations 7 and 8 are situated close to the STF in the SAZ. At both stations, the samples include Subantarctic Surface Water (SASW), SAMW (potential density $\sigma_\theta \sim 26.8$ kg/m^3) and samples from below the SAMW layer with a contribution of AAIW ($\sigma_\theta \sim 27.3$ kg/m^3) (Talley et al., 2011; Table 1, Fig. 1b). Station 9 shows potential temperature (θ) – salinity (S) characteristics typical of the PFZ with a zigzagging pattern related to the mixing of southerly and northerly waters (Talley et al., 2011). The deepest sample has similar θ-S properties as further deep samples obtained at stations 10 and 20 close to the density level of UCDW ($\sigma_\theta \sim 27.6$ kg/m^3, Fig. 1b).

Station 10 and stations 18 and 20 in the Drake Passage are all situated south of the PF in the AZ based on the temperature minimum associated with Antarctic Surface Water (ASW) referred to as Winter Water (Fig. 1b, Talley et al., 2011). Surface waters to a maximal depth of 150 m at station 20, hence, represent ASW, including its coldest form, Winter Water (Fig. 1b). Below this depth, the water column is occupied by UCDW evidenced by an O_2-minimum situated at ~250 m at station 10 and 18 and at ~800 m at station 20. The deepest samples at station 10 and 18 are close to or within the salinity maximum of LCDW ($\sigma_\theta \sim 27.8$ kg/m^3).

Similar θ-S properties as at stations 10, 18 and 20 are also observed at stations 14 and 15 in the Subpolar Region neighbouring the Balleny Islands, although the temperature minimum associated with Winter Water is less pronounced (Fig. 1b) and UCDW is absent south of the southern boundary of the ACC (Orsi et al., 1995). Station 12 close to Antarctica shows nearly homogenous temperatures throughout the water column at variable salinities. The deepest samples, denser than ASW, represent modified LCDW (Whitworth et al., 1998) and are overlain by waters that are somewhat colder than ASW at the more northerly stations (Fig. 1b).

2.3. Biogeochemical processes in the Southern Ocean

The spatial nutrient distribution and regimes of nutrient limitation are closely associated with ocean circulation patterns and biogeochemical dynamics as surface waters are transported away from upwelling sites. Waters north of the STF are characterized by generally low macronutrient concentrations, while higher concentrations are characteristic of the SAZ and AZ, where biological productivity is primarily limited by iron (Fe) (e.g. Martin et al., 1990; Boyd et al., 2007; Moore et al., 2013 and references therein).

In addition to these large-scale oceanic nutrient dynamics, Fe supply from sea ice (e.g. Lannuzel et al., 2016), terrestrial sources close to the Antarctic continent (e.g. Death et al., 2014) and subantarctic islands (e.g. Blain et al., 2007), as well as mesoscale eddies (Jones et al., 2017), transiently relax Fe-limitation of phytoplankton growth. While these mesoscale features directly impact the biological community and the biogeochemical cycles of major and micronutrients, recent data demonstrate that not all biologically-cycled elements are affected in terms of concentrations and/or isotope compositions (e.g. Wang et al., 2019).

In recent years, a range of stable isotope systems have been studied in the Southern Ocean (e.g. de Souza et al., 2012; Abouchami et al., 2014; Zhao et al., 2014; Sieber et al., 2019, Wang et al., 2019) in order to constrain the effects of Southern Ocean biological processes on their spatial distributions and with the perspective of applying these tools to reconstruct biogeochemical conditions in the past. Silicon (Si) and cadmium (Cd) show very similar patterns (de Souza et al., 2012; Abouchami et al., 2014; Sieber et al., 2019). Both are strongly depleted in surface waters of the AZ and PFZ due to biological uptake resulting in heavy isotope signatures that are incorporated into SAMW/AAIW and become easily traceable features at intermediate depths in adjacent ocean basins. Although zinc (Zn) also shows strong surface depletions, there is very little expression of this in terms of Zn isotope variability (Zhao et al., 2014; Wang et al., 2019). Contrasting with Si, Cd and Zn, Ni neither shows strong surface depletions nor large isotopic variability with depth (Cameron and Vance, 2014; Wang et al., 2019). Notably, all four elements are very homogenous in their isotope compositions at depths below AAIW.

Our ACE samples include a north-south transect across nutrient regimes as well as stations near the ice-edge and downstream of isolated islands, allowing the cycling of Cr to be investigated in these varied and dynamic environments. In addition, as subsurface waters exported from the Southern Ocean are known to be important contributors to the distribution and depth profile structure of macronutrients (Sarmiento et al., 2004), trace metals (Frew and Hunter, 1992; de Souza et al., 2018) and metal isotopes (Abouchami et al., 2014; Sieber et al., 2019), our ACE samples can give insight into deep water Cr and δ^{53}Cr that will be useful in constraining Cr cycling in the global ocean.

3. METHODS

3.1. Sample collection

A trace metal clean rosette system (General Oceanics) equipped with 10 l Niskin-X bottles was used to collect sea-

water samples. The bottles were transferred to a class 100 clean container aboard the ship and seawater was filtered through pre-rinsed Supor Acropak capsule filters (0.2 μm) collecting aliquots in 1 l LDPE Nalgene bottles. The bottles were cleaned successively for >7 days in RBS detergent and then for >7 days in 10% HCl p.a., including extensive intermediate and final rinses with MilliQ water (18.2 MΩ/cm resistivity). Samples were acidified to pH ≤ 2 with double distilled HCl and double bagged for transport and storage at room temperature at the University of Bern.

3.2. Chromium stable isotope measurements

3.2.1. Preliminary chromium concentrations

Initial Cr concentrations, to ensure the addition of appropriate amounts of Cr double spike, were determined on 30 ml sample aliquots. To this end, 0.2 ml 5 ppb ^{50}Cr spike was added to 30 ml of seawater. Subsequently, Cr was enriched from solution by co-precipitation with $Mg(OH)_2$ through the addition of 0.7 ml of ammonia solution (Romil UpA, assay 20–22%) (e.g. Semeniuk et al., 2016). After centrifugation and removal of the supernatant, the precipitate was dissolved in 2 ml 1 M HNO_3, transferred to Teflon vials and evaporated to dryness. Separation of Cr from Mg, Ti and V was achieved on cation columns with 1 ml resin bed, whereby the sample was loaded in 1 M HNO_3 (Yamakawa et al., 2009). The natural Cr concentration was determined by MC-ICP-MS (Neptune Plus, Thermo Fisher). Measured ^{52}Cr/^{50}Cr ratios were corrected for machine mass bias by a simplified standard-sample-bracketing approach (e.g. Albarède et al., 2004), applying the mass bias deduced from an unspiked NIST 979 standard run once every 6 samples. Mass bias corrected ratios were converted to Cr concentrations by standard isotope dilution equations (e.g. Stracke et al., 2014).

3.2.2. Spiking and purification of 1 l isotope samples

Appropriate amounts of ^{50}Cr-^{54}Cr double spike (338 ppb, in 2 M HNO_3) were added to 1 l seawater samples for Cr isotope determinations, targeting a molar Cr spike proportion of 0.5 of the total Cr in the sample-spike mixture (see Section 3.2.4). All samples were stored for several months at pH ≤ 2, ensuring that all Cr was present as Cr (III) (e.g. Jeandel and Minster, 1987; Semeniuk et al., 2016). Spiked samples were left for equilibration for >48 h before the precipitation of $Mg(OH)_2$ was induced by adding 5–6 ml ammonia solution to yield a pH of 10–11. For OSIL water (used as an internal standard, see Section 3.2.4), the needed volume corresponded to 10 ml. A large fraction of the supernatant was poured off two days after precipitation. Further separation of the precipitate was achieved by centrifugation. The precipitate was eventually dissolved in 4–6 ml 4 M HCl and transferred to Teflon vials. Half a millilitre 30% H_2O_2 (Romil UpA) was added to oxidize organic compounds and the samples were refluxed at 110 °C for >48 h. The sample solutions were finally dried and immediately taken up in 9 ml 0.022 M HCl in preparation for the first chromatographic column. Alternatively, the oxidizing step used 1 ml concentrated HNO_3. In this case, the samples were converted back to Cl-form prior to the dissolution in 9 ml dilute HCl employing two repetitions of dissolution and drying in 1–2 ml of 6 M HCl.

The two-step chromatographic purification followed previously established methods. Chromium was first loaded as Cr(VI) on an anion column in dilute HCl (2 ml resin bed, AG 1-X8, 100–200 mesh) to remove the Mg-matrix and further elements (e.g. Ball and Bassett, 2000). For the oxidation of Cr, 1 ml of 0.2 M ammonium persulfate (TCI chemicals) was added to the 9 ml of sample solution and the sample boiled for 1 h at 130 °C. Samples were subsequently loaded at room temperature and Cr purification accomplished as outlined in Table 2a. The visible residue of the first column is a sulphur-rich brown dot. This residue was dissolved in 3 ml 1 M HNO_3 and processed through a cation column (1 ml resin bed, AG 50W-X8, 200–400 mesh) using an elution scheme adapted from Yamakawa et al. (2009, see Table 2b). This scheme included a step of Fe elution in 0.5 M HF, which resulted in final ^{56}Fe/(^{54}Cr+^{54}Fe) ratios <0.03 appropriate for analysis by MC-ICP-MS (see Section 3.2.4).

In general, the protocol outlined above is similar to the procedure reported by Moos and Boyle (2019). We have not observed any detectable polyatomic sulfur interferences on mass 49 after the use of ammonium-persulfate and

Table 2
(a) Ion chromatographic scheme for the separation of Cr from major elements, especially Mg, and Ti, V and Fe on 2 ml of anion resin (AG 1-X8, 100–200 mesh, adapted from Schoenberg et al., 2008). (b) Final purification of Cr from S and residual Ti, V and Fe on 1 ml of cation resin (AG 50W-X8, 200–400 mesh, modified from Yamakawa et al., 2009). For more details see Section 3.2.2.

(a) Anion column		(b) Cation column	
Clean	15 ml 1 M HNO_3	Clean	7 ml 6.4 M HCl
Condition	2 × 2 ml 0.02 M HCl		7 ml 0.5 M HF
		Condition	2 × 1 ml 1 M HNO_3
Load sample	in 9 ml 0.022 M HCl/		
(at room temperature)	1 ml 0.2 M ammonium persulfate	Load sample	in 3 ml 1 M HNO_3
		(after 4 days in this acid at room temperature)	
Elute matrix	20 ml 0.1 M HCl		
incl. Ti, V and Fe	10 ml MQ	Elute residual Ti, V and S	7 ml 1 M HNO3
		Elute residual Fe	7 ml 0.5 M HF
Collect Cr	2 × 1 ml 1 M HNO3	Elute residual Mg	3 × 8 ml 1 M HCl
	wait 1.5 hours	Collect Cr	7 ml 2 M HCl
	3 × 4 ml 1 M HNO3		

cation resin (c.f. Moos and Boyle, 2019), in agreement with other studies reporting Cr isotope data obtained by MC-ICP-MS (e.g. Schoenberg et al., 2008). Notably, Schoenberg et al. (2008) report that many of their samples were run directly after the anion column involving ammonium-persulfate.

3.2.3. Procedural yields and blanks

The procedural yields, inferred from observed ^{52}Cr signals compared to signals expected from sample Cr concentrations, range between 34% and 70%, with an average of 53%, similar to those reported by Moos and Boyle (2019). In general, it would be valuable to constrain the cause of these relatively low yields, since improvements would allow processing smaller seawater samples in the future. In principle, they could result from variable yields during Cr co-precipitation with $Mg(OH)_2$ performed for relatively large water volumes and/or variable recoveries during ion chromatography. Our column calibrations suggested Cr recovery of >90% for the anion column and >99% for the cation column. However, since the calibrations were performed with mixtures of Ti, V, Cr and Fe only, it is not clear if the high column recoveries can also be expected for the processed seawater matrices. The yields are not of analytical concern given that blank to sample ratios remained <1.5% as detailed below.

The advantage of pre-concentrating Cr with $Mg(OH)_2$ is the low associated blank. In contrast to Cr enrichment with added Fe(II) (Bonnand et al., 2013; Scheiderich et al., 2015; Goring-Harford et al., 2018), Mg is naturally present in seawater and only ammonia solution (<0.1 pmol Cr per ml) is needed for the enrichment. Iron(II), on the other hand, can contribute large amounts of Cr with variable Cr isotope compositions (320 pmol Cr per sample, Goring-Harford et al., 2018). In each series of 11 samples, one procedural blank was obtained starting with the transfer of 6 ml of 4 M HCl from a centrifuge tube to a Teflon vial (see above) and continuing the procedure as for the samples. The observed blanks ranged between 12.5 and 16.3 pmol (14.4 ± 1.4 pmol, 1 SD, n = 6). To assess the contributions to the procedural blank from the anion column, the ammonium – persulfate and the cation column, we processed pure reagents through the columns. The anion column was run with and without the oxidising agent, and its blank was deduced from the difference between these runs. The results indicate that ~83% of the procedural blank stems from the anion column, most of which is from the ammonium – persulfate (~80% of ~83%), while the cation column contributes ~17%. The procedural blanks are negligible and correspond to 0.9% on average and a maximum of 1.5% of sample derived Cr. Whether variable procedural blanks affect the data quality has been assessed through replicate measurements of seawater samples and seawater salinity standards (OSIL water) described in the next section.

3.2.4. Chromium mass spectrometry

3.2.4.1. Double spike isotope composition and concentration. The Cr double spike was prepared from enriched ^{50}Cr and ^{54}Cr obtained in metal form from Isoflex. Both single spikes contained substantial amounts of Fe, and, as a consequence, they were purified separately on anion resin (e.g. Scheiderich et al., 2015). Single spikes were mixed in appropriate proportions to yield optimal ^{54}Cr and ^{50}Cr abundances following Rudge et al. (2009). The double spike was calibrated for its isotope composition by running several NIST 979 double spike mixtures with a molar spike Cr proportion between 0.15 and 0.6 and optimizing the composition to yield $\delta^{53}Cr = 0$ across the range. The calibration gave isotope compositions of 41.9997, 1.4666 and 29.2410 for ^{50}Cr/^{52}Cr, ^{53}Cr/^{52}Cr and ^{54}Cr/^{52}Cr, respectively, relative to internally normalized values of 0.051859 (reference ratio, Birck and Allègre, 1984), 0.113456 and 0.028208 for NIST 979. The calibration reveals no significant trend for the δ^{53}Cr – value of NIST 979 in the range of the described mixtures.

The uncertainty on the natural mass fractionation factor based on the chosen double spike composition is relatively constant and minimal in a range of molar Cr spike proportions between 0.1 and 0.6, with an absolute minimum at ~0.3 (Rudge et al., 2009), although the model does not consider any interferences. Due to the interference correction of ^{54}Fe on ^{54}Cr, and initial observations on internal errors in function of spike proportion, we decided to measure samples at a spike proportion of ~0.5 (spike Cr/sample Cr = 1). This yields larger ^{54}Cr signals, which are less affected by uncertainties of the ^{54}Fe interference correction. As a result of the accurate available preliminary Cr concentrations, samples were run at nearly constant spike proportions between 0.48 and 0.53.

The Cr double spike has been calibrated for its concentration in mixtures with a solution of known Cr concentration. This Cr solution was prepared from a pure Cr metal grain digest (99.995% Cr, Alfa Aesar). The error on the concentration calibration is <0.3% based on the weighing uncertainty during digestion and subsequent dilutions.

3.2.4.2. MC-ICP-MS setup and measuring sequences. Solutions were introduced in 0.5 M HNO_3 using an Aridus II desolvating system (Cetac) and a Savillex nebulizer with a nominal uptake rate of 100 µl/min. Mounted cones consisted of a standard sample cone and an X skimmer cone. The cup-configuration included cups equipped with 10^{11} Ω resistors for the four Cr isotopes (50, 52, 53 and 54) and interfering elements monitored by ^{49}Ti, ^{51}V and ^{56}Fe. Titanium and V interfere on ^{50}Cr, while Fe interferes on ^{54}Cr. Interference levels of these elements after the two-stage purification scheme were negligible and corrected for as detailed below. Chromium was measured in medium resolution on the ArC-, ArO- and ArN-free low mass shoulder at a mass setting of 51.91–51.913 for the axial ^{52}Cr cup depending on the session (e.g. Schoenberg et al., 2008; Goring-Harford et al., 2018). The signals of the Ar-species were reduced avoiding the use of nitrogen as a sweep gas and using a torch position relatively distant from the sample cone (z typically at around −2 mm). Usual signals with this setup were 17–20 V of (natural) ^{52}Cr for a 70 ppb solution. Background levels in 0.5 M HNO_3 were <0.4 mV ^{49}Ti, <1 mV ^{51}V, 5–10 mV ^{52}Cr and <8 mV ^{56}Fe. There was a slight tendency for ^{52}Cr to increase in the course of a session, usually starting at ~5 mV and ending at ~10 mV.

Sample and standard measurements consisted of 36 × 4.2 s of beam integration. Between analyses the system was rinsed with a first wash solution for 70 s, and a second wash and an on-peak background solution for 18 × 4.2 s each. The average on-peak background preceding a sample or standard measurement was subtracted from the raw intensities of samples and standards prior to data reduction.

Before running samples and NIST 979 – double spike mixtures, a set of 6 pure internally normalized NIST 979 standards were run to verify stable machine performance. Subsequently, three NIST 979 – double spike mixtures were measured and evaluated for their δ^{53}Cr. Alternating measurements of three samples and one NIST 979 – double spike mixture followed these pre-measurements to allow, if needed, for drift correction. No drift occurred in any of the sessions of this study, and the sample data were corrected with the session's average deviation of all NIST 979 – double spike mixtures from 0. This deviation was ≤0.025‰ in absolute terms, with 2 SD ≤ 0.023‰ and 2 SEM ≤ 0.007‰, each session including at least nine measurements of the standard. Given the homogenous spiking of samples, NIST 979 – double spike mixtures were only run at a spike proportion of ~0.5 identical to the samples.

3.2.4.3. Data reduction and interference levels of Ti, V and Fe. The Cr isotope composition of samples and standards was deduced from raw background-corrected intensities in a R-script following Rudge et al. (2009). The equations were complemented and include interference corrections for Ti, V and Fe on Cr assuming the same machine fractionation for these elements as for Cr and natural isotope compositions.

Maximal observed ^{49}Ti/cup50, ^{51}V/cup50 and ^{56}Fe/cup54 ratios in the samples were 2×10^{-5}, 9×10^{-5} and 0.03, respectively. The average sample ^{56}Fe/cup54 was 0.011. Given natural ^{50}Ti/^{49}Ti = 0.9725, ^{50}V/^{51}V = 0.0246 and ^{54}Fe/^{56}Fe = 0.0637, this implies that Fe was by far the largest interference constituting up to 2.1×10^{-3} of the 54 beam, compared to maximal proportions of 2×10^{-5} and 2×10^{-6} of Ti and V on cup 50. Based on this, we investigated the tolerance for Fe interference corrections running NIST 979 – double spike mixtures with added Fe yielding a ^{56}Fe/cup54 ratio of 0.04. For the data reduction we assumed light Fe (δ^{56}Fe = −5), unfractionated Fe (δ^{56}Fe = 0, ^{56}Fe/^{54}Fe = 1/0.0637) and heavy Fe (δ^{56}Fe = +5) to be contained in the sample. The assumption of unfractionated Fe yielded δ^{53}Cr values as for the Fe-free runs, and differed by 0.005 δ-units for the other cases. The uncertainty induced due to the interference correction of Fe is therefore small, corresponding to a fraction of the internal errors of sample measurements ranging between 0.02 and 0.03 δ-units (2 SEM, Table 1). This finding is in agreement with Bonnand et al. (2011), who also concluded that residual Fe in samples at levels similar to those observed here are easily correctable.

3.2.4.4. Accuracy and precision of δ^{53}Cr and Cr concentrations. Internal errors of the sample measurements provide an optimistic estimate of the precision of isotope and concentration data, as they do not monitor any issues potentially arising from variable chemical blank contributions, changing mass spectrometric conditions from session to session and/or inaccurate sample and double spike weighing. As already noted, internal errors range between ±0.02 and ±0.03‰ for δ^{53}Cr (2 SEM) for measurements at natural ^{52}Cr beam sizes between 11 and 24 V, with an average of 19 V. Internal errors of concentration measurements deduced from the double spike data reduction are not relevant, since they are orders of magnitude smaller than anticipated errors from double spike and sample weighing.

A more realistic estimate of the precision of our data has been obtained through separate processing of several aliquots of three different batches of OSIL water and of two duplicates from the ACE cruise (Table 3). OSIL is a commercially available salinity standard (35 psu) collected from the surface ocean near the Sargasso Sea (http://www.osil.co.uk). To ensure sample-spike equilibration, OSIL waters

Table 3
Chromium data for OSIL waters and ACE samples processed as full replicates. The listed recommended values are based on replicate measurements at the Saskatchewan Isotope Laboratory obtained by TIMS. Error estimates derived from this data set correspond to ±0.036‰ for δ^{53}Cr and to ±2.2% for Cr concentration (2 SD, see Section 3.2.4.4).

	Origin (Osil Batch date)	This study Cr (nmol/kg)	δ^{53}Cr	2 SEM	Recommended values Cr (nmol/kg)	2 SD	δ^{53}Cr	2 SD	n
OSIL	Saskatchewan Isotope Laboratory (2/9/2015)	4.38	0.68	0.03	4.27	0.02	0.66	0.01	4
		4.22	0.66	0.02					
OSIL	Saskatchewan Isotope Laboratory (16/9/2015)	3.23	0.97	0.03	3.30	0.08	0.97	0.01	2
		3.24	0.95	0.02					
OSIL	University of Bern (5/12/2017)	4.03[a]	0.85	0.03					
		3.99[a]	0.82	0.02					
		4.05[a]	0.86	0.02					
		4.19[b]	0.85	0.02					
		4.18[b]	0.83	0.03					
ACE replicates									
TM 9–50 m		3.44	0.95	0.03					
		3.44	0.99	0.02					
TM 10–80 m		3.75	0.91	0.02					
		3.73	0.92	0.02					

[a] Bottle 1.
[b] Bottle 2.

were acidified to a pH < 2 and left for more than a month before processing (see Section 3.2.2). Different batches are not identical in terms of Cr concentrations and isotopes (Scheiderich et al., 2015; Paulukat et al., 2016; Goring-Harford et al., 2018), which renders the standard less valuable for our purpose.

We also noted a small but consistent offset in the Cr concentration of OSIL waters from the same batch, but taken from two different purchased 5 l bottles (Table 3, OSIL 5/12/2017). This observation has been confirmed by further measurements of aliquots from the second bottle, which were processed (and will be reported) in the context of a new study. Hence, we treat these bottles as separate samples when estimating the precision of Cr isotopes and concentrations from the compilation of duplicate and triplicate measurements in Table 3. The standard deviation for δ^{53}Cr is calculated from the formula $SD^2 = 1/k\Sigma_i d_i^2$, where d_i is the deviation in δ^{53}Cr of a sample from the corresponding mean of replicate measurements and k is the number of degrees of freedom equal to the difference between the number of analyses and the number of samples (Kenney and Keeping, 1951, Chapter, 7.11). Analogously, the relative standard deviation for concentrations is calculated from the relative deviation of each measured sample concentration from the respective mean concentration. The derived error for δ^{53}Cr corresponds to ±0.036‰ and to ±2.2% for Cr concentrations (2 SD in both cases, based on 13 measurements of 6 samples).

The Saskatchewan Isotope Laboratory (C. Holmden) provided two OSIL batches that were processed as full duplicates. Our measured isotope compositions for these samples deviate by at most 0.02 δ-units from the values obtained by the Saskatchewan Isotope Laboratory (measured by TIMS). The maximal difference for concentration data corresponds to 2.7% (Table 3).

4. RESULTS

4.1. Dissolved chromium concentrations

Dissolved Cr concentrations show only subtle variations with depth at each station, with slight depletion in the surface compared to deeper waters (Fig. 2a, Table 1). The gradient is particularly small at stations 8, 10, 12, 14, 15 and 18 where the increase with depth ranges between 3 and 5%. A somewhat larger increase is observed at stations 7, 9 and 20 with Cr subsurface enrichments ranging between 7 and 11%.

Chromium concentrations systematically increase from north to south (Fig. 2a). Average Cr concentrations correspond to 3.32 and 3.25 nmol/kg at station 7 and 8 in the SAZ, 3.49 at station 9 in the PFZ, and 3.78 at stations 10 and 12 along the transect from Tasmania to Antarctica. Further southerly sites – 14, 15, 18 and 20 – yield very similar average Cr concentrations to those observed at stations 10 and 12 ranging between 3.71 and 3.84 nmol/kg.

4.2. Dissolved chromium isotope compositions

Overall, the observed variability in Cr isotope compositions is within 0.2 δ-units, between δ^{53}Cr = +0.87‰ (station 18, 180 m) and +1.06‰ (station 8, 150 m, Table 1). As for Cr concentrations, station-specific variations in δ^{53}Cr are small, usually much smaller than the maximal observed range of 0.1 δ-units at station 9 (Fig. 2b). At all but three sites, these variations remain within analytical uncertainty (2 SD = 0.036 δ-units, Section 3.2.4.4). Station 7 and 9 (2 SD = 0.06‰), and to a lesser degree station 20 (2 SD = 0.04‰), show larger variability trending towards lower δ^{53}Cr values at depth. Chromium isotope compositions vary from north to south, similar to Cr concentrations (Fig. 2b): stations 7, 8 in the SAZ yield average δ^{53}Cr of +1.03‰ (±0.02, 2 SEM) and +1.04‰ (±0.01), respectively, somewhat higher than station 9 in the PFZ (+0.97 ± 0.02‰). All other more southerly sites are nearly identical with average values between +0.89 and +0.92‰ (2 SEM = ±0.01 to 0.02).

4.3. Relationship between chromium concentrations and isotope compositions

Previous studies have revealed a tight relationship between dissolved Cr concentrations and isotope compositions in open-ocean samples (Scheiderich et al., 2015; Goring-Harford et al., 2018; Moos and Boyle, 2019). The compiled literature data, excluding coastal waters showing freshwater influence (Scheiderich et al., 2015), samples with relatively imprecise Cr concentrations (10–15% uncertainty, Paulukat et al., 2016), and analyses of isolated seawater samples (Economou-Eliopoulos et al., 2016; Pereira et al., 2016; Holmden et al., 2016; Farkaš et al., 2018; Frei et al., 2018), are consistent with a Rayleigh-type fractionation of Cr in a closed system, yielding an isotopic enrichment factor of $\varepsilon = -0.82 \pm 0.09$‰ (2 SD, n = 81, $R^2 = 0.79$). The new data from this study are consistent with these earlier observations with a calculated ε of -0.82 ± 0.06‰ (2 SD, n = 66, $R^2 = 0.92$). A fit to all data yields $\varepsilon = -0.81 \pm 0.06$‰ (2 SD, n = 147, $R^2 = 0.83$, Fig. 3a).

Chromium seawater data, where concentrations and isotopes are available, range between 1.2 and 6.5 nmol/kg and between +0.41 and +1.72‰ in δ^{53}Cr (Fig. 3a). Samples from the Arctic and the Atlantic Ocean (Scheiderich et al., 2015; Goring-Harford et al., 2018) yield generally heavier Cr isotope compositions than those observed in the Southern Ocean, with the exception of the data reported from the Argentine Basin (δ^{53}Cr = +0.41 to +0.66‰, Bonnand et al., 2013). Seawater δ^{53}Cr in the range of the Southern Ocean or even lighter are observed at the SAFe station in the subtropical North Pacific (δ^{53}Cr = +0.68 to +1.11‰, Moos and Boyle, 2019) and in the northeast Pacific (station PAPA, δ^{53}Cr = +0.61 and +0.91‰, Scheiderich et al., 2015).

5. DISCUSSION

5.1. Potential effects of elemental inputs from Antarctica and the Balleny Islands

Terrestrial input may influence Cr and δ^{53}Cr distributions at coastal stations, either through direct Cr inputs

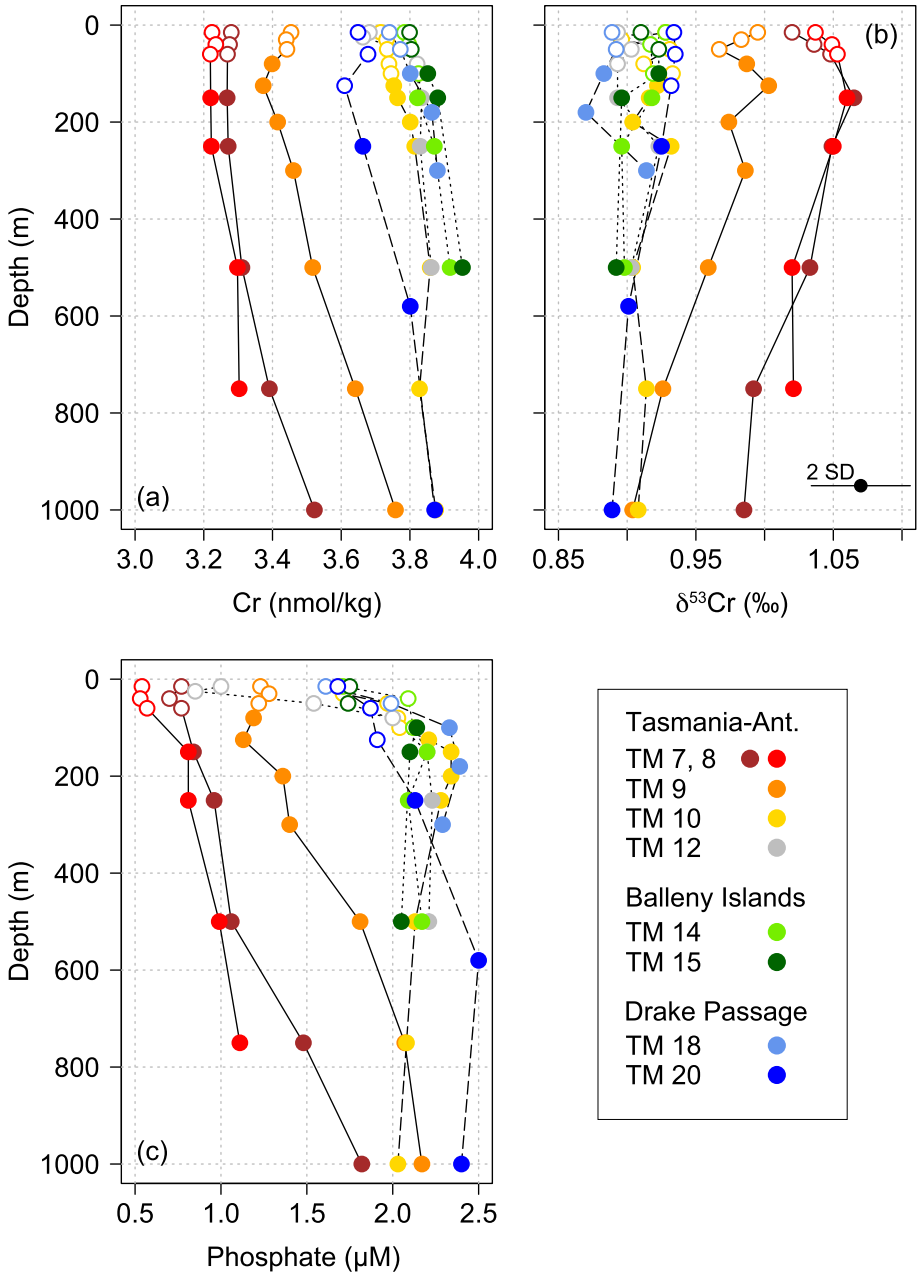

Fig. 2. Depth profiles of Cr concentrations (a), δ^{53}Cr (b) and phosphate (c). Chromium concentrations increase southwards, while δ^{53}Cr values decrease. Open circles represent surface waters (ASW, SASW), filled circles all deeper water masses.

or secondary effects from inputs of other elements that could affect the biogeochemical cycling of Cr. Iron, for instance, is supplied to the surface ocean downstream of oceanic islands (e.g. Blain et al., 2007) as well as adjacent to Antarctica by subglacial meltwater and icebergs (e.g. Death et al., 2014; Lannuzel et al., 2016), fuelling phytoplankton blooms. Similarly, Si is released from glacial sediments shed into the surface ocean by subglacial meltwater or released from iceberg hosted glacial debris (Hawkings et al., 2017). Basaltic islands, such as the Ballenys, are not strongly enriched in Cr compared to the continental crust (249 versus 92 ppm, Gale et al., 2013; Rudnick and Gao, 2014). However, basaltic rocks are relatively reactive in seawater (e.g. Pearce et al., 2013) and easily weathered (Dessert et al., 2003), which could lead to detectable concentration and isotopic shifts for Cr. Such island-derived Cr could, hence, be associated with particulate and dissolved freshwater fluxes from the islands, but also reflect seawater-basalt interactions along the coast.

Inputs from landmasses occur at the Mertz Glacier station close to Antarctica (station 12), at both sites neighbouring the Balleny Islands (stations 14 and15) and close

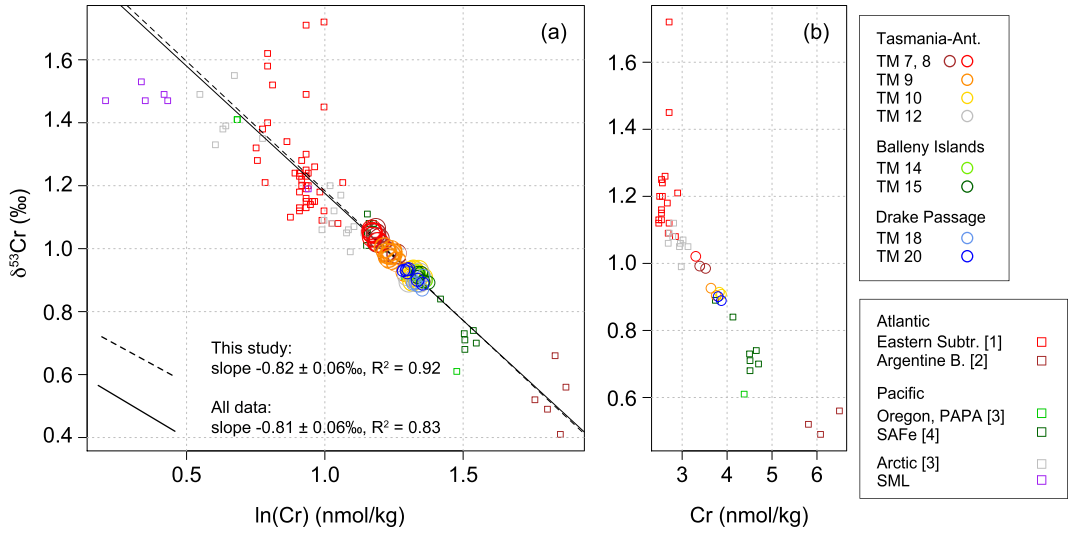

Fig. 3. (a) δ^{53}Cr versus ln(Cr) for the new data from the Southern Ocean and data in the literature: [1] Goring-Harford et al. (2018); [2] Bonnand et al. (2013); [3] Scheiderich et al. (2015); [4] Moos and Boyle (2019). The new data and all data taken together yield similar slopes with corresponding isotopic enrichment factors for Cr of $\varepsilon = -0.82$ and -0.81‰, respectively (both ±0.06‰, 2 SD). Surface Mixed Layer samples from the Arctic are diluted by melt or river water and are, hence, not included in the regression (see Scheiderich et al., 2015). (b) shows the same data as (a) but for deep waters only (>500 m). Chromium concentrations increase from the Atlantic to the Pacific Ocean with δ^{53}Cr becoming gradually lighter.

to the western Antarctic Peninsula (station 18), based on elevated Si relative to nitrate (Fig. 4). None of these sites, however, shows particularly high Cr concentrations and/or lowered δ^{53}Cr (Fig. 2), which would hint at a significant terrestrial Cr source. Furthermore, these stations are virtually identical to the open ocean stations south of the PF in terms of Cr isotopes and concentrations (stations 10 and 20, Fig. 2). In summary, the impact of terrestrial fluxes on Cr and its isotopes seems insignificant at these sites adjacent to the coast.

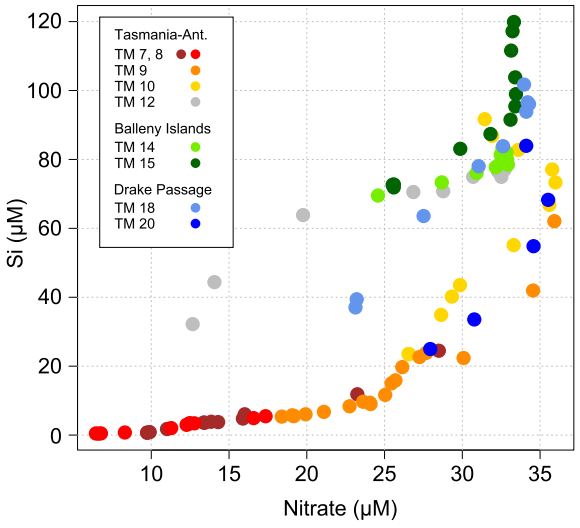

Fig. 4. Silicon versus nitrate for the studied stations. Data represent all sampled depths, contrasting with the Cr data, where only a subset is available at each site (Table 1; Hassler and Ellwood, 2019). Station 12 close to the Mertz Glacier, stations 14 and 15 adjacent to the Balleny Islands, and station 18 on the western Antarctic Peninsula, show strong deviations from the relationship between both nutrients observed elsewhere. This relative enrichment in Si is interpreted to reflect inputs from neighbouring landmasses.

5.2. Cycling of Cr in the Southern Ocean

Active biological uptake of (micro-) nutrients leads to nutrient type depth profiles characterized by relative surface water depletion and subsurface enrichment (e.g. Bruland et al., 2014). If an element is not of immediate biological need, it can still be enriched at depth through particulate scavenging in the surface ocean and release during remineralization (e.g. Bruland et al., 2014). In contrast to other transitional metals such as Mn, Fe, Ni, Co, Cu, Zn and Mo (e.g. Morel et al., 2014), there is at present no documentation of a specific metabolic function of Cr in marine phytoplankton. Phytoplankton culture experiments suggest that reduced Cr(III) can be adsorbed and to a lesser degree taken up by phytoplankton, which may explain some of the seawater variability in dissolved Cr concentrations and δ^{53}Cr (Semeniuk et al., 2016).

Biological processes, including scavenging, active uptake and remineralization, should affect Cr and δ^{53}Cr most markedly in surface waters. At the southerly stations 10, 14, 15, 18 and 20 phosphate is depleted by 12–20% in the shallow samples taken at 15 m water depth compared to Winter Water (Fig. 2c), which reflects the phosphate concentration in the well-mixed winter surface layer. Comparing the same samples for Cr indicates surface depletions of at most 1.4% (Fig. 2a, Table 1). Station 12, in turn, shows an even stronger phosphate depletion of 50% between the surface and 80 m, resulting from enhanced biological productivity near Mertz Glacier, while the concomitant Cr

depletion of 4% is consistent with dilution by glacial melt (Fig. 1b, Table 1). All of these observations suggest that biologically driven drawdown of Cr in the surface ocean is very subtle at these southerly sites, much lower than for major nutrients. This finding is also consistent with Cr isotopes, which do not show significant variations with depth (Fig. 2b).

Similar considerations for stations 7 and 8 in the SAZ are less meaningful based on the available data. Sampled SASW is from very similar densities at both stations (Fig. 1b). Hence, nutrients and Cr concentrations are expected to be well-mixed, consistent with observations (Fig. 2a, c). At sampled depth close to the SAMW pycnostat (Fig. 1b), Cr and phosphate concentrations are influenced by advection with SAMW, such that Cr profiles are unlikely to reflect local removal and remineralization processes.

Taken together, the data provide no evidence for strong removal and isotope fractionation of Cr in the surface of the Southern Ocean by scavenging and/or active biological uptake. A similar observation has recently been made for Ni and its isotopes close to the Kerguelen Plateau, where Ni shows only a subtle depletion of up to ~5% between the surface and 200 m, with no change in Ni isotope compositions (Wang et al., 2019).

5.3. Water mass mixing

The relevance of mixing is most evident by looking at the distribution of Cr and its isotopes in relation to isopycnals along which mixing primarily occurs. There are three main observations regarding Cr isotopes (Fig. 5b): (i) The variability at all sites south of the PF, stations 10–20, is very limited such that all observations fall into the analytical confidence interval around the mean isotope composition at these sites ($\delta^{53}Cr = +0.91 \pm 0.036‰$). (ii) Deviations from this range are limited to station 9 in the PFZ, and stations 7 and 8 in the SAZ. (iii) At the level of SAMW and below at stations 7–9, $\delta^{53}Cr$ gradually changes towards the southerly range in Cr isotope compositions.

These observations are mirrored in Cr concentrations (Fig. 5a). Lower Cr concentrations are observed in surface waters for stations 7–9, increasing towards southerly values further down the water column.

The first observation (i) is in agreement with the statements on vertical Cr cycling in Section 5.2. Antarctic Surface Water is not distinct in terms of $\delta^{53}Cr$ from underlying CDW, which precludes significant surficial fractionation of Cr after its supply to the surface ocean by upwelling CDW. However, concentrations below Winter Water gradually increase with depth (Fig. 5a). This pattern is consistent with the mixing of Winter Water with slightly Cr enriched CDW also indicated by θ and S (Fig. 1b). The slight enrichment in Cr of CDW relative to ASW likely implies a time-integrated effect of vertical Cr redistribution by particles, which is however very subtle and not expressed in a clear drawdown and fractionation of Cr in ASW.

The data also indicate that Cr isotopes are not distinct between UCDW and LCDW (Fig. 5b). If there are any differences in Cr isotope compositions in the source waters from the Atlantic, Indian and Pacific Ocean, which are not evenly represented in Upper and Lower CDW (Talley

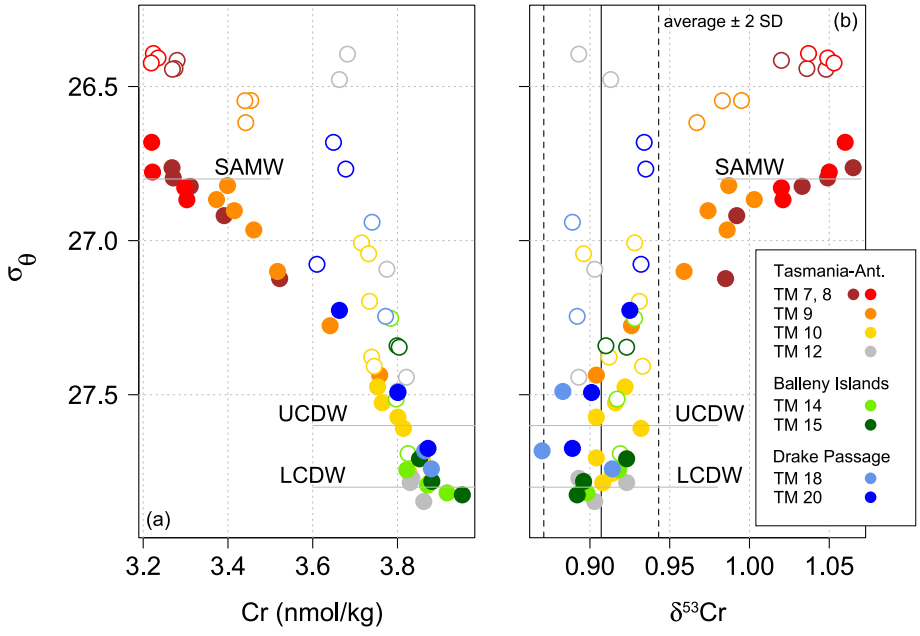

Fig. 5. Chromium concentration (a) and isotope profiles (b) with respect to potential density σ_0. $\delta^{53}Cr$ is very homogenous at stations 10–20 south of the PF, all observations are within the analytical uncertainty of the mean ($+0.91 \pm 0.036‰$, shown as solid an dashed lines). Deviations from this range and clearly lower Cr concentrations are observed in the PFZ at station 9 and in the SAZ at station 7 and 8. Open circles represent surface waters (ASW, SASW), filled circles all deeper water masses. Isopycnals are labelled at the cores of intermediate and deep water masses ($\sigma_{0,SAMW} \sim 26.8$, $\sigma_{0,UCDW} \sim 27.6$ and $\sigma_{0,LCDW} \sim 27.8$ kg/m^3).

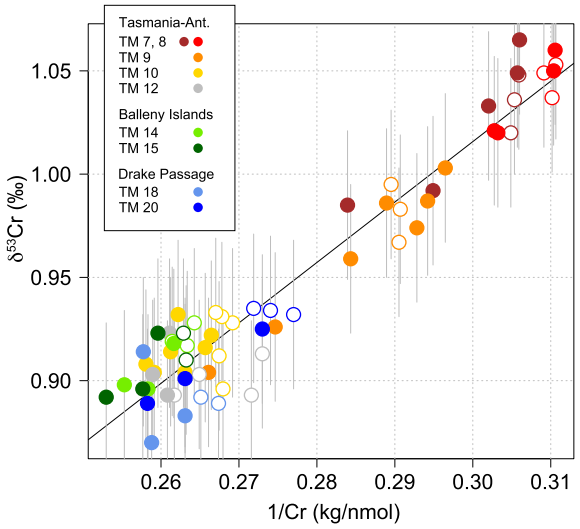

Fig. 6. δ^{53}Cr versus 1/Cr for all studied samples. The strong correlation indicates that all observations can be viewed as a mixture of two end-members ($R^2 = 0.93$, $p < 0.001$). This interpretation is hydrographically meaningful for station 9 in the PFZ, where the Cr concentrations and isotope compositions result from mixing of waters from either side of the zone. Further aspects of this correlation in the context of physical mixing are discussed in Section 5.3. Open circles represent surface waters (ASW, SASW), filled circles all deeper water masses.

et al., 2011), they do not appear to be large enough to impose variability between these water masses.

Observation (ii) can, in principle, be explained in two ways. Either the different Cr systematics north of the PF reflect specific Cr fractionation processes at these sites, or, alternatively, mixing of southerly Cr isotope compositions with a heavier signature generated northward of the studied sites. δ^{53}Cr versus 1/Cr indicates that all data can be viewed as a mixture between two end-members of distinct Cr characteristics (Fig. 6). Hydrographically, it is clear that station 9 in the PFZ is a mixture of waters from both sites of this zone (Fig. 1b, Section 2.2), providing the physical framework to explain Cr at station 9 in terms of mixing. As an extension of this concept, Cr and δ^{53}Cr are shown for all samples in two potential density intervals relevant for stations 7–9 (Fig. 7). The shallow samples ($\sigma_\theta < 26.6$ kg/m^3), as well as the underlying waters surrounding the SAMW pycnostat of ~26.8 ($26.7 < \sigma_\theta < 27.1$), reveal a strong linear relationship between salinity and Cr, as well as between salinity and δ^{53}Cr ($R^2 > 0.84$ for all regressions, Fig. 7). This suggests that not only station 9 in the PFZ, but also station 7 and 8 in SAZ, reflect different mixtures of southerly waters and an isotopically heavier northerly source. The origin of this northerly source is discussed in Section 5.4.

Lastly, it should be noted that the shift towards southerly Cr concentrations and isotope compositions for the

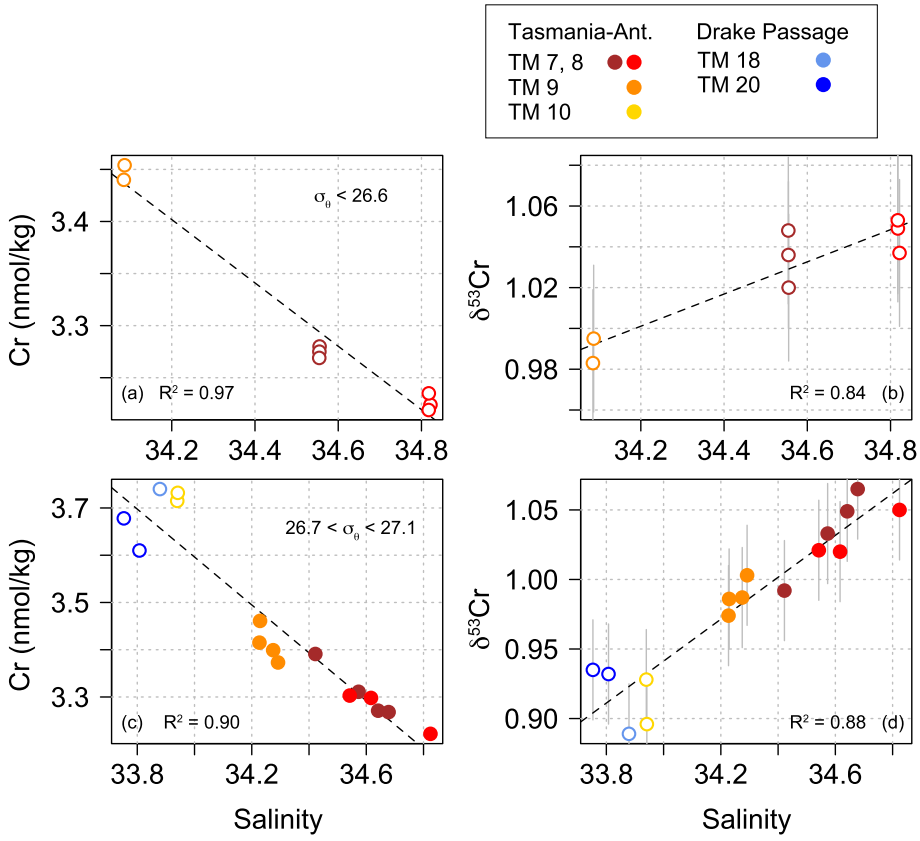

Fig. 7. Cr and δ^{53}Cr versus salinity for surface waters (a, b) and waters surrounding the SAMW pycnostat (c, d). All relationships yield high R^2 values suggesting that mixing in these layers controls the Cr distribution. Open circles represent surface waters (ASW, SASW), filled circles all deeper water masses.

deepest samples at stations 7 and 9 ($\sigma_\theta > 27.1$), observation (iii), is consistent with hydrographic properties of these waters which trend towards the density of UCDW (Fig. 5) and the respective θ-S characteristic (Fig. 1b).

5.4. Origin of the Cr isotope variability

Although mixing may primarily explain the spatial distribution of Cr concentrations and isotope compositions in the study area, the process(es) that generate isotopically heavy Cr signatures north of the SAZ, remain unidentified as yet. On the one hand, this signature may be generated as a result of the cycling of Cr within the subtropical gyre, perhaps associated with the drawdown of major nutrients. Alternatively, it could also reflect Cr removal in oxygen minimum zones (Rue et al., 1997), the signature of which could subsequently be mixed into the subtropical gyre. Whether the effects of oxygen minimum zones on Cr cycling can be significant enough is questionable. At present, there is little evidence for strong removal and fractionation of Cr in such zones (Goring-Harford et al., 2018; Moos and Boyle, 2019).

In support of Cr isotope fractionation as a result of major nutrient drawdown, a relatively strong linear relationship between δ^{53}Cr and phosphate is observed for the stations of this study (Fig. 8). Phosphate and nitrate show a coherent linear relationship for the studied sites ($R^2 = 0.97$) and, as a result, their relationships with δ^{53}Cr are very similar. At present, it seems premature to assign a causal link to these relationships, because they could essentially result from the mixing of low and high latitude waters characterized by opposing nutrient contents and

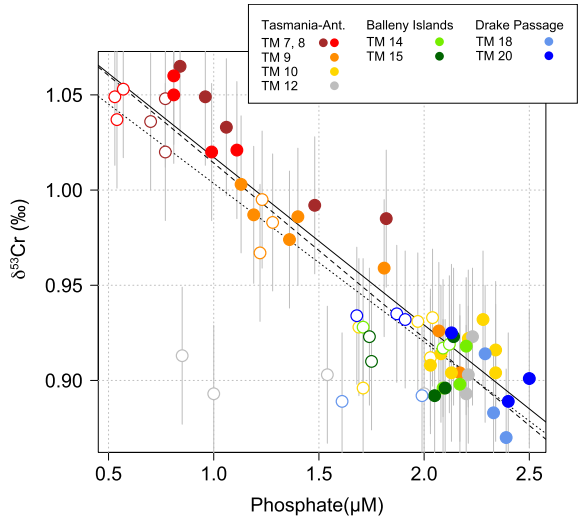

Fig. 8. δ^{53}Cr versus phosphate for all studied sites. Linear regressions are shown to all data (dotted line, $R^2 = 0.72$), all data excluding station 12 close to Mertz Glacier (dashed, $R^2 = 0.85$), and to the stations which are not influenced by the coast (station 7, 8, 9, 10, 20, see Section 5.1, solid $R^2 = 0.88$). The relationship results from the strong meridional gradient in phosphate, dominating over variations in the water column at each site, coupled to the systematic change in δ^{53}Cr with latitude. For more details see Section 5.4. Open circles represent surface waters (ASW, SASW), filled circles all deeper water masses.

Cr isotope composition (Section 5.3), without Cr fractionation being induced by nutrient utilization. Two aspects should be noted: Firstly, the relationship between phosphate and δ^{53}Cr is weak at individual sites. While phosphate shows surface depletions, δ^{53}Cr is virtually invariant with depth (Fig. 2a, c; Section 5.2). The relationship, hence, reflects the strong meridional gradient in phosphate coupled to the meridional change in δ^{53}Cr, rather than a common cycling of Cr with nutrients at any specific site. Second, the relationship is strongly improved if station 12 at the Mertz Glacier is not considered, whereby R^2 increases from 0.72 to 0.85. The stronger surface depletion of phosphate at this station cannot result from glacial dilution based on salinity. Instead it likely reflects enhanced biological productivity, which, however, does not affect Cr isotopes appreciably at this site (Fig. 8).

5.5. Global variability of δ^{53}Cr

A linear regression fitting δ^{53}Cr as a function of 1/Cr for the global data set suggests that seawater can be explained in terms of mixing between two end members ($R^2 = 0.80$, not shown, fit to the same data as in Fig. 3a). Such a scenario seems very unlikely, since it implies two distinct, probably riverine, sources of Cr to seawater (also see the discussion in Scheiderich et al., 2015). Alternatively, adhering to mixing, one might argue that any continental flux could be characterized by a systematic relationship of Cr concentration and δ^{53}Cr, consistent with the overall mixing line. Concentrations of Cr in rivers are, however, strongly affected by Cr abundance in drained lithologies (McClain and Maher, 2016), while the dissolved isotope composition reflects redox conditions in river catchments (D'Arcy et al., 2016). Hence, a well defined relationship in rivers seems unlikely, such that the overall distribution of Cr and its isotopes in seawater more likely reflects internal cycling governed by a very consistent fraction of $\varepsilon = -0.81 \pm 0.06$‰. This does, however, not preclude that mixing of water masses governs the seawater Cr concentration and δ^{53}Cr composition on a regional scale as argued for the data presented here (Section 5.3).

As noted previously (Scheiderich et al., 2015), the relatively small isotope fractionation of Cr inferred from the global seawater data set is somewhat unexpected, given that most known Cr reducing agents induce much larger isotopic shifts (see Section 1). In principle, there are (at least) four reasons to explain this apparent discrepancy, but we currently have little constraints to favour one of them over the others. First, it could imply that the observed isotope fractionation does not only reflect Cr reduction, but instead is also significantly influenced by sorption of Cr(VI) with minimal fractionation (Ellis et al., 2004). Second, it may imply that Cr isotope fractionation in the marine realm is small because of reduction in low oxygen settings. Small Cr isotope fractionation has been observed for soil bacteria under denitrifying conditions ($\varepsilon = -0.4 \pm 0.2$‰, Han et al., 2012). Third, it could be related to Cr reduction kinetics whereby faster reduction leads to lowered fractionation (e.g. Sikora et al., 2008; Wanner and Sonnenthal, 2013; Jamieson-Hanes et al., 2014). Fourth, it could reflect that

Cr(VI) reduction mostly takes place within surface sediments, resulting in an effective isotope fractionation factor that is smaller than the intrinsic one (e.g. Clark and Johnson, 2008; Wanner and Sonnenthal, 2013).

Contrary to Si, Zn or Cd (e.g. de Souza et al., 2012; Zhao et al., 2014; Wang et al., 2019; Sieber et al., 2019), Cr shows limited nutrient-like behaviour in the Southern Ocean. In a similar manner, Cr also reveals a relatively limited enrichment in deep waters from the Atlantic to the Pacific Ocean by a factor of ~2 (depth >500 m, Fig. 3b), contrasting with enrichments of ~18 and ~10 for Si and Zn, respectively (e.g. Bruland et al., 2014). Nevertheless, the deep-water Cr data show a relatively consistent increase in concentrations and a decrease in δ^{53}Cr from the Atlantic through the Southern Ocean into the Pacific (Fig. 3b). The global deep water pattern may, hence, primarily reflect continuous small additions of a regenerated Cr pool (see also Jeandel and Minster, 1987), which is isotopically light due to the removal of reduced Cr(III) at shallow depths, possibly coupled with the sorption of Cr(VI) onto particles.

The seawater data from the Argentine Basin (Bonnand et al., 2013) are exceptional, as they are lower in δ^{53}Cr and Cr-richer compared to data from the Pacific. However, it may be that they are not representative of the true seawater signal since these water samples were not filtered (Goring-Harford et al., 2018). A further unusual observation concerns UCDW sampled in the Equatorial Atlantic with $\delta^{53}Cr = +1.72‰$ (Goring-Harford et al., 2018). Upper Circumpolar Deep Water reported in the present study is much lower ($+0.90 \pm 0.05‰$, 2 SD, Table 1), meaning that the isotope composition of UCDW appears to be altered strongly during transit from the Southern Ocean, accompanied by less significant Cr removal. This heavy signature of UCDW is, however, unique at this stage and awaits confirmation.

6. CONCLUSIONS

This study presents the first stable seawater Cr isotope data from the Southern Ocean in an attempt to further our understanding of the biogeochemical cycling of Cr. The studied sites include a north-south, cross-frontal transect from south of Tasmania to Mertz Glacier in Antarctica, two stations adjacent to the Balleny Islands and two stations in the Drake Passage. The cross-frontal transect sheds light on the behaviour of Cr and its isotopes under different nutrient conditions, while stations adjacent to Antarctica and the basaltic Balleny Islands, provide insight into coastal Cr sources and/or coastal processes, which could affect the biogeochemical cycling of Cr in the water column.

Although a coastal influence is clearly identifiable in the Si-nitrate relationship at four sites, namely the Mertz Glacier, the Balleny Island stations and close to the western Antarctic Peninsula, seawater δ^{53}Cr and Cr concentrations remain unaffected. Hence, neither glacial meltwater and debris, nor seawater–basalt interactions supply significant amounts of Cr. Elemental fluxes from land also do not appear to affect Cr cycling by indirect means, for instance through the stimulation of primary productivity. As at the coastal sites, Cr depletion and isotopic shifts are also absent in Antarctic and Subantarctic Surface Waters of the open ocean. Biological uptake of Cr, or scavenging of Cr onto particles in the surface of the Southern Ocean, is apparently not significant enough for such depletion to occur. Nevertheless, time-integrated vertical redistribution of Cr likely causes the relatively subtle enrichment of Cr in Circumpolar Deep Water compared to Antarctic Surface Water.

Contrasting with the small variations in δ^{53}Cr and Cr concentrations at each site, there is systematic north-south variability in both parameters. Seawater samples, from the uppermost 1000 m of the water column, show an increase in Cr concentrations and a decrease in δ^{53}Cr from the Subantarctic across the Polar Frontal into the Antarctic Zone. South of the Polar Front, Cr concentrations and isotopes are, however, very similar at all sites. This latitudinal variability is consistent with mixing of waters as evidenced by strong correlations of Cr and δ^{53}Cr with salinity in a density interval around Subantarctic Mode Water and at shallower depth. At present, the mechanism that generates heavier δ^{53}Cr at lower latitudes remains uncertain. It may either be related to a change in Cr cycling under macronutrient depleted conditions in the subtropics or originate from the reduction of Cr in oxygen deficient zones.

Consistent with earlier work, the new data also reveal a strong relationship between Cr concentrations and δ^{53}Cr. All presently available data define an apparent fractionation of Cr in seawater with $\varepsilon = -0.81 \pm 0.06‰$, assuming a closed system Rayleigh type fractionation. Internal cycling of Cr in the oceans likely generates this overall relationship, rather than mixing of riverine inputs with well-defined Cr-δ^{53}Cr systematics. The process(es) that lead to remarkably well-defined Cr systematics in seawater are not well-constrained as yet and need to be investigated in detail in the future. Specifically, such work should investigate seawater Cr isotopes at oxygen levels lower than in the settings studied so far and in settings with contrasted biological productivity of the surface ocean. Further relevant insights are likely to be gained through the study of particulate Cr fractions.

ACKNOWLEDGEMENTS

This work was supported by the Swiss National Science Foundation (SNSF – grant PP00P2_172915). It forms part of project 15 of the Antarctic Circumnavigation Expedition, a scientific expedition carried out under the auspices of the Swiss Polar Institute (SPI), supported by funding from the ACE Foundation and Ferring Pharmaceuticals. We are grateful to the Chief Scientist, the late David Walton, the captain and the crew of the R/V *Akademik Tryoshnikov* for their support during the voyage. We also thank Jenny Thomas (SPI, data manager). The MC-ICP-MS at the Institute of Geological Sciences, University of Bern was acquired within the framework of the NCCR project PlanetS. We acknowledge Robert Steel, Simone Moos and Martin Wille for sharing analytical expertise, Martin also for everyday support on the mass spectrometer. Philipp Nasemann contributed two OSIL analyses that were also obtained at the University of Bern with the same methods outlined in this study. Gregory de Souza, Matthias Sieber, Philipp Nasemann, Christoph Wanner and Derek Vance are acknowledged

for discussions and comments. Lastly, we thank two anonymous reviewers and the associate editor, Rachael James, for their comprehensive and valuable comments.

REFERENCES

Abouchami W., Galer S. J. G., De Baar H. J. W., Middag R., Vance D., Zhao Y., Klunder M., Mezger K., Feldmann H. and Andreae M. O. (2014) Biogeochemical cycling of cadmium isotopes in the Southern Ocean along the Zero Meridian. *Geochim. Cosmochim. Acta* **127**, 348–367.

Albarède F., Telouk P., Blichert-Toft J., Boyet M., Agranier A. and Nelson B. (2004) Precise and accurate isotopic measurements using multiple-collector. *Geochim. Cosmochim. Acta* **68**, 2725–2744.

Ball J. W. and Bassett R. L. (2000) Ion exchange separation of chromium from natural water matrix for stable isotope mass spectrometric analysis. *Chem. Geol.* **168**, 123–134.

Basu A., Johnson T. M. and Sanford R. A. (2014) Cr isotope fractionation factors for Cr(VI) reduction by a metabolically diverse group of bacteria. *Geochim. Cosmochim. Acta* **142**, 349–361.

Bauer K. W., Gueguen B., Cole D. B., Francois R., Kallmeyer J., Planavsky N. and Crowe S. A. (2018) Chromium isotope fractionation in ferruginous sediments. *Geochim. Cosmochim. Acta* **223**, 198–215.

Birck J.-L. and Allègre C. J. (1984) Chromium isotopic anomalies in Allende Refractory Inclusions. *Geophys. Res. Lett.* **11**, 943–946.

Blain S., Quéguiner B., Armand L., Belviso S., Bombled B., Bopp L., Bowie A., Brunet C., Brussaard C., Carlotti F., Christaki U., Corbière A., Durand I., Ebersbach F., Fuda J. L., Garcia N., Gerringa L., Griffiths B., Guigue C., Guillerm C., Jacquet S., Jeandel C., Laan P., Lefèvre D., Lo Monaco C., Malits A., Mosseri J., Obernosterer I., Park Y. H., Picheral M., Pondaven P., Remenyi T., Sandroni V., Sarthou G., Savoye N., Scouarnec L., Souhaut M., Thuiller D., Timmermans K., Trull T., Uitz J., Van Beek P., Veldhuis M., Vincent D., Viollier E., Vong L. and Wagener T. (2007) Effect of natural iron fertilization on carbon sequestration in the Southern Ocean. *Nature* **446**, 1070–1074.

Bonnand P., James R. H., Parkinson I. J., Connelly D. P. and Fairchild I. J. (2013) The chromium isotopic composition of seawater and marine carbonates. *Earth Planet. Sci. Lett.* **382**, 10–20.

Bonnand P., Parkinson I. J., James R. H., Karjalainen A. M. and Fehr M. A. (2011) Accurate and precise determination of stable Cr isotope compositions in carbonates by double spike MC-ICP-MS. *J. Anal. At. Spectrom.* **26**, 528–535.

Boyd P. W., Jickells T., Law C. S., Blain S., Boyle E. A., Buesseler K. O., Coale K. H., Cullen J. J., de Baar H. J. W., Follows M., Harvey M., Lancelot C., Levasseur M., Owens N. P. J., Pollard R., Rivkin R. B., Sarmiento J., Schoemann V., Smetacek V., Takeda S., Tsuda A., Turner S. and Watson A. J. (2007) Mesoscale iron enrichment experiments 1993–2005: synthesis and future directions. *Science* **315**, 612–617.

Bruland K. W., Middag R. and Lohan M. C. (2014) 8.2 – Controls of trace metals in seawater. In *Treatise on Geochemistry (Second Edition)* (eds. H. D. Holland and K. K. Turekian). Elsevier, Oxford, pp. 19–51.

Cameron V. and Vance D. (2014) Heavy nickel isotope compositions in rivers and the oceans. *Geochim. Cosmochim. Acta* **128**, 195–211.

Clark S. K. and Johnson T. M. (2008) Effective isotopic fractionation factors for solute removal by reactive sediments: a laboratory microcosm and slurry study. *Environ. Sci. Technol.* **42**, 7850–7855.

Connelly D. P., Statham P. J. and Knap A. H. (2006) Seasonal changes in speciation of dissolved chromium in the surface Sargasso Sea. *Deep Sea Res. Part I* **53**, 1975–1988.

Crowe S. A., Døssing L. N., Beukes N. J., Bau M., Kruger S. J., Frei R. and Canfield D. E. (2013) Atmospheric oxygenation three billion years ago. *Nature* **501**, 535–538.

D'Arcy J., Babechuk M. G., Døssing L. N., Gaucher C. and Frei R. (2016) Processes controlling the chromium isotopic composition of river water: constrains from basaltic river catchments. *Geochim. Cosmochim. Acta* **186**, 296–315.

Death R., Wadham J. L., Monteiro F., Le Brocq A. M., Tranter M., Ridgwell A., Dutkiewicz S. and Raiswell R. (2014) Antarctic ice sheet fertilises the Southern Ocean. *Biogeosciences* **11**, 2635–2643.

de Souza G. F., Khatiwala S. P., Hain M. P., Little S. H. and Vance D. (2018) On the origin of the marine zinc–silicon correlation. *Earth Planet. Sci. Lett.* **492**, 22–34.

de Souza G. F., Reynolds B. C., Johnson G. C., Bullister J. L. and Bourdon B. (2012) Silicon stable isotope distribution traces Southern Ocean export of Si to the eastern South Pacific thermocline. *Biogeosciences* **9**, 4199–4213.

Dessert C., Dupré B., Gaillardet J., François L. M. and Allègre C. J. (2003) Basalt weathering laws and the impact of basalt weathering on the global carbon cycle. *Chem. Geol.* **202**, 257–273.

Døssing L. N., Dideriksen K., Stipp S. L. S. and Frei R. (2011) Reduction of hexavalent chromium by ferrous iron: a process of chromium isotope fractionation and its relevance to natural environments. *Chem. Geol.* **285**, 157–166.

Economou-Eliopoulos M., Frei R. and Megremi I. (2016) Potential leaching of Cr(VI) from laterite mines and residues of metallurgical products (red mud and slag): an integrated approach. *J. Geochem. Explor.* **162**, 40–49.

Ellis A. S., Johnson T. M. and Bullen T. D. (2002) Chromium isotopes and the fate of hexavalent chromium in the environment. *Science* **295**, 2060–2062.

Ellis A. S., Johnson T. M. and Bullen T. D. (2004) Using chromium stable isotope ratios to quantify Cr(VI) reduction: lack of sorption effects. *Environ. Sci. Technol.* **38**, 3604–3607.

Farkaš J., Chrastný V., Novák M., Čadkova E., Pašava J., Chakrabarti R., Jacobsen S. B., Ackerman L. and Bullen T. D. (2013) Chromium isotope variations (δ53/52Cr) in mantle-derived sources and their weathering products: implications for environmental studies and the evolution of δ53/52Cr in the Earth's mantle over geologic time. *Geochim. Cosmochim. Acta* **123**, 74–92.

Farkaš J., Frýda J., Paulukat C., Hathorne E. C., Matoušková Š., Rohovec J., Frýdová B., Francová M. and Frei R. (2018) Chromium isotope fractionation between modern seawater and biogenic carbonates from the Great Barrier Reef, Australia: implications for the paleo-seawater δ53Cr reconstruction. *Earth Planet. Sci. Lett.* **498**, 140–151.

Fendorf S. E. (1995) Surface-reactions of chromium in soils and waters. *Geoderma* **67**, 55–71.

Frei R., Gaucher C., Poulton S. W. and Canfield D. E. (2009) Fluctuations in Precambrian atmospheric oxygenation recorded by chromium isotopes. *Nature* **461**, 250–253.

Frei R., Paulukat C., Bruggmann S. and Klaebe R. M. (2018) A systematic look at chromium isotopes in modern shells-implications for paleo-environmental reconstructions. *Biogeosciences* **15**, 4905–4922.

Frei R., Poiré D. and Frei K. M. (2014) Weathering on land and transport of chromium to the ocean in a subtropical region

(Misiones, NW Argentina): a chromium stable isotope perspective. *Chem. Geol.* **381**, 110–124.

Frew R. D. and Hunter K. A. (1992) Influence of Southern Ocean waters on the cadmium–phosphate properties of the global ocean. *Nature* **360**, 144–146.

Gale A., Dalton C. A., Langmuir C. H., Su Y. and Schilling J. G. (2013) The mean composition of ocean ridge basalts. *Geochem. Geophys. Geosyst.* **14**, 489–518.

Goring-Harford H. J., Klar J. K., Pearce C. R., Connelly D. P., Achterberg E. P. and James R. H. (2018) Behaviour of chromium isotopes in the eastern sub-tropical Atlantic Oxygen Minimum Zone. *Geochim. Cosmochim. Acta* **236**, 41–59.

Gueguen B., Reinhard C. T., Algeo T. J., Peterson L. C., Nielsen S. G., Wang X., Rowe H. and Planavsky N. J. (2016) The chromium isotope composition of reducing and oxic marine sediments. *Geochim. Cosmochim. Acta* **184**, 1–19.

Han R., Qin L., Brown S. T., Christensen J. N. and Beller H. R. (2012) Differential isotopic fractionation during Cr(VI) reduction by an aquifer-derived bacterium under aerobic versus denitrifying conditions. *Appl. Environ. Microbiol.* **78**, 2462–2464.

Hassler C. and Ellwood M. (2019) Nutrient concentration in seawater samples, collected from the underway supply, CTD and trace metal rosettes in the Southern Ocean during the austral summer of 2016/2017, on board the Antarctic Circumnavigation Expedition (ACE). (Version 1.0). Zenodo. doi: 10.5281/zenodo.2616606.

Hawkings J. R., Wadham J. L., Benning L. G., Hendry K. R., Tranter M., Tedstone A., Nienow P. and Raiswell R. (2017) Ice sheets as a missing source of silica to the polar oceans. *Nat. Commun.* **8**, 14198.

Henry T., Robinson C., Haumann F.A., Thomas J., Hutchings J., Schuback N., Tsukernik M. and Leonard K. (2019) Physical and biogeochemical oceanography from Conductivity, Temperature, Depth (CTD) rosette deployments during the Antarctic Circumnavigation Expedition (ACE). (Version 1.0). Zenodo. doi: 10.5281/zenodo.3247384.

Holmden C., Jacobson A. D., Sageman B. B. and Hurtgen M. T. (2016) Response of the Cr isotope proxy to Cretaceous Ocean Anoxic Event 2 in a pelagic carbonate succession from the Western Interior Seaway. *Geochim. Cosmochim. Acta* **186**, 277–295.

Jamieson-Hanes J. H., Lentz A. M., Amos R. T., Ptacek C. J. and Blowes D. W. (2014) Examination of Cr(VI) treatment by zero-valent iron using in situ, real-time X-ray absorption spectroscopy and Cr isotope measurements. *Geochim. Cosmochim. Acta* **142**, 299–313.

Jeandel C. and Minster J. F. (1987) Chromium behavior in the ocean: global versus regional processes. *Global Biogeochem. Cycles* **1**, 131–154.

Jones E. M., Hoppema M., Strass V., Hauck J., Salt L., Ossebaar S., Klaas C., van Heuven S. M. A. C., Wolf-Gladrow D., Stöven T. and de Baar H. J. W. (2017) Mesoscale features create hotspots of carbon uptake in the Antarctic Circumpolar Current. *Deep Sea Res. Part II* **138**, 39–51.

Kenney J. and Keeping E. (1951) Mathematics of statistics, second ed., vol. 2. D. Van Nostrand Company, Inc., p. 162 (Chapter 7.11).

Kitchen J. W., Johnson T. M., Bullen T. D., Zhu J. and Raddatz A. (2012) Chromium isotope fractionation factors for reduction of Cr(VI) by aqueous Fe(II) and organic molecules. *Geochim. Cosmochim. Acta* **89**, 190–201.

Lannuzel D., Vancoppenolle M., Van Der Merwe P., De Jong J., Meiners K. M., Grotti M., Nishioka J. and Schoemann V. (2016) Iron in sea ice: review & new insights. *Elementa* **4**, 130.

Martin J. H., Fitzwater S. E. and Gordon R. M. (1990) Iron deficiency limits phytoplankton growth in Antarctic waters. *Global Biogeochem. Cycles* **4**, 5–12.

McClain C. N. and Maher K. (2016) Chromium fluxes and speciation in ultramafic catchments and global rivers. *Chem. Geol.* **426**, 135–157.

Miller C. A., Peucker-Ehrenbrink B., Walker B. D. and Marcantonio F. (2011) Re-assessing the surface cycling of molybdenum and rhenium. *Geochim. Cosmochim. Acta* **75**, 7146–7179.

Moore C. M., Mills M. M., Arrigo K. R., Berman-Frank I., Bopp L., Boyd P. W., Galbraith E. D., Geider R. J., Guieu C., Jaccard S. L., Jickells T. D., La Roche J., Lenton T. M., Mahowald N. M., Marañón E., Marinov I., Moore J. K., Nakatsuka T., Oschlies A., Saito M. A., Thingstad T. F., Tsuda A. and Ulloa O. (2013) Processes and patterns of oceanic nutrient limitation. *Nat. Geosci.* **6**, 701–708.

Moos S. B. and Boyle E. A. (2019) Determination of accurate and precise chromium isotope ratios in seawater samples by MC-ICP-MS illustrated by analysis of SAFe Station in the North Pacific Ocean. *Chem. Geol.* **511**, 481–493.

Morel F. M. M., Milligan A. J. and Saito M. A. (2014) 8.5 – Marine bioinorganic chemistry: the role of trace metals in the oceanic cycles of major nutrients. In *Treatise on Geochemistry (Second Edition)* (eds. H. D. Holland and K. K. Turekian). Elsevier, Oxford, pp. 123–150.

Orsi A. H., Johnson G. C. and Bullister J. L. (1999) Circulation, mixing, and production of Antarctic Bottom Water. *Prog. Oceanogr.* **43**, 55–109.

Orsi A. H., Whitworth, III, T. and Nowlin, Jr, W. D. (1995) On the meridional extent and fronts of the Antarctic Circumpolar Current. *Deep-Sea Res. Part I* **42**, 641–673.

Paulukat C., Gilleaudeau G. J., Chernyavskiy P. and Frei R. (2016) The Cr-isotope signature of surface seawater—a global perspective. *Chem. Geol.* **444**, 101–109.

Pearce C. R., Jones M. T., Oelkers E. H., Pradoux C. and Jeandel C. (2013) The effect of particulate dissolution on the neodymium (Nd) isotope and Rare Earth Element (REE) composition of seawater. *Earth Planet. Sci. Lett.* **369–370**, 138–147.

Pereira N. S., Voegelin A. R., Paulukat C., Sial A. N., Ferreira V. P. and Frei R. (2016) Chromium-isotope signatures in scleractinian corals from the Rocas Atoll, Tropical South Atlantic. *Geobiology* **14**, 54–67.

Planavsky N. J., Reinhard C. T., Wang X., Thomson D., McGoldrick P., Rainbird R. H., Johnson T., Fischer W. W. and Lyons T. W. (2014) Low mid-proterozoic atmospheric oxygen levels and the delayed rise of animals. *Science* **346**, 635–638.

Reinhard C. T., Planavsky N. J., Wang X., Fischer W. W., Johnson T. M. and Lyons T. W. (2014) The isotopic composition of authigenic chromium in anoxic marine sediments: a case study from the Cariaco Basin. *Earth Planet. Sci. Lett.* **407**, 9–18.

Rickli J., Janssen D.J., Hassler C., Ellwood M. and Jaccard S.L. (2019) Seawater chromium concentrations and isotope compositions in the Southern Ocean during the austral summer of 2016/2017, on board the Antarctic Circumnavigation Expedition (ACE). (Version 1.0). Zenodo. doi: 10.5281/zenodo.3250980.

Rudge J. F., Reynolds B. C. and Bourdon B. (2009) The double spike toolbox. *Chem. Geol.* **265**, 420–431.

Rudnick R. L. and Gao S. (2014) 4.1 – Composition of the continental crust. In *Treatise on Geochemistry (Second Edition)* (eds. H. D. Holland and K. K. Turekian). Elsevier, Oxford, pp. 1–51.

Rue E. L., Smith G. J., Cutter G. A. and Bruland K. W. (1997) The response of trace element redox couples to suboxic conditions in the water column. *Deep Sea Res. Part I* **44**, 113–134.

Saleh F. Y., Parkerton T. F., Lewis R. V., Huang J. H. and Dickson K. L. (1989) Kinetics of chromium transformations in the environment. *Sci. Total Environ.* **86**, 25–41.

Sarmiento J. L., Gruber N., Brzezinski M. A. and Dunne J. P. (2004) High-latitude controls of thermocline nutrients and low latitude biological productivity. *Nature* **427**, 56–60.

Scheiderich K., Amini M., Holmden C. and Francois R. (2015) Global variability of chromium isotopes in seawater demonstrated by Pacific, Atlantic, and Arctic Ocean samples. *Earth Planet. Sci. Lett.* **423**, 87–97.

Schlitzer R. (2019) Ocean Data View, <https://odv.awi.de>.

Schoenberg R., Zink S., Staubwasser M. and von Blanckenburg F. (2008) The stable Cr isotope inventory of solid Earth reservoirs determined by double spike MC-ICP-MS. *Chem. Geol.* **249**, 294–306.

Semeniuk D. M., Maldonado M. T. and Jaccard S. L. (2016) Chromium uptake and adsorption in marine phytoplankton – Implications for the marine chromium cycle. *Geochim. Cosmochim. Acta* **184**, 41–54.

Sieber M., Conway T. M., de Souza G. F., Obata H., Takano S., Sohrin Y. and Vance D. (2019) Physical and biogeochemical controls on the distribution of dissolved cadmium and its isotopes in the Southwest Pacific Ocean. *Chem. Geol.* **511**, 494–509.

Sikora E. R., Johnson T. M. and Bullen T. D. (2008) Microbial mass-dependent fractionation of chromium isotopes. *Geochim. Cosmochim. Acta* **72**, 3631–3641.

Sirinawin W., Turner D. R. and Westerlund S. (2000) Chromium (VI) distributions in the Arctic and the Atlantic Oceans and a reassessment of the oceanic Cr cycle. *Mar. Chem.* **71**, 265–282.

Stracke A., Scherer E. E. and Reynolds B. C. (2014) 15.4 – Application of isotope dilution in geochemistry. In *Treatise on Geochemistry (Second Edition)* (eds. H. D. Holland and K. K. Turekian). Elsevier, Oxford, pp. 71–86.

Talley L. D., Pickard G. L., Emery W. J. and Swift J. H. (2011) Chapter 13 – Southern Ocean. In *Descriptive Physical Oceanography* (eds. L. D. Talley, G. L. Pickard, W. J. Emery and J. H. Swift), sixth ed. Academic Press, Boston, pp. 437–471.

van der Weijden C. H. and Reith M. (1982) Chromium(III) — chromium(VI) interconversions in seawater. *Mar. Chem.* **11**, 565–572.

Wang R. M., Archer C., Bowie A. R. and Vance D. (2019a) Zinc and nickel isotopes in seawater from the Indian Sector of the Southern Ocean: the impact of natural iron fertilization versus Southern Ocean hydrography and biogeochemistry. *Chem. Geol.* **511**, 452–464.

Wang X., Glass J. B., Reinhard C. T. and Planavsky N. J. (2019b) Species-dependent chromium isotope fractionation across the eastern tropical north pacific oxygen minimum zone. *Geochem. Geophys. Geosyst.* **20**, 2499–2514.

Wanner C. and Sonnenthal E. L. (2013) Assessing the control on the effective kinetic Cr isotope fractionation factor: a reactive transport modeling approach. *Chem. Geol.* **337–338**, 88–98.

Wei W., Frei R., Chen T. Y., Klaebe R., Liu H., Li D., Wei G. Y. and Ling H. F. (2018) Marine ferromanganese oxide: a potentially important sink of light chromium isotopes? *Chem. Geol.* **495**, 90–103.

Whitfield M. and Turner D. R. (1987) The role of particles in regulating the composition of seawater. In *Aquatic Surface Chemistry* (ed. W. Stumm). Wiley-Interscience, New York, pp. 457–493.

Whitworth T., Orsi A.H., Kim S.-J. and Nowlin W.D. (1998) Water Masses and Mixing Near the Antarctic Slope Front, in: Jacobs, S.S., Weiss, R.F. (Eds.), Ocean, Ice, and Atmosphere: Interactions at the Antarctic Continental Margin, pp. 1–27.

Yamakawa A., Yamashita K., Makishima A. and Nakamura E. (2009) Chemical separation and mass spectrometry of Cr, Fe, Ni, Zn, and Cu in terrestrial and extraterrestrial materials using thermal ionization mass spectrometry. *Anal. Chem.* **81**, 9787–9794.

Zhao Y., Vance D., Abouchami W. and de Baar H. J. W. (2014) Biogeochemical cycling of zinc and its isotopes in the Southern Ocean. *Geochim. Cosmochim. Acta* **125**, 653–672.

Zink S., Schoenberg R. and Staubwasser M. (2010) Isotopic fractionation and reaction kinetics between Cr(III) and Cr(VI) in aqueous media. *Geochim. Cosmochim. Acta* **74**, 5729–5745.

Associate editor: Rachael James